

HYDROMAGNETIC FLOW AROUND THE MAGNETOSPHERE

John R. Spreiter, Audrey L. Summers,
and Alberta Y. Alksne

National Aeronautics and Space Administration
Space Sciences Division
Ames Research Center
Moffett Field, Calif.

PRICE \$

PRICE(S) \$

Hard copy (HC) 2.00

Microfiche (MF) .75

18351

Abstract — A magnetohydrodynamic model for the interaction of the solar wind and the geomagnetic field is described, the degree to which the governing equations may be approximated by the simpler equations of the classical Chapman-Ferraro theory combined with gasdynamics is examined, and numerical results for a number of representative cases are presented. In the hydromagnetic model, the magnetosphere boundary and distant tail are represented by tangential and contact discontinuities, and the bow wave by a fast hydromagnetic shock wave. The connectivity of interplanetary and geomagnetic fields, and the asymptotic directions of the wake and shock waves at great distances from the earth are discussed in terms of properties of these discontinuities. Detailed numerical results for the location of the bow wave, and the density, velocity, and temperature of the flow in the region between the bow wave and the magnetosphere are presented for Mach numbers 5, 8, and 12 for $\gamma = 5/3$ and 2. The calculated position of the bow wave is shown to be in good accordance with that observed in shadowgraph photographs of supersonic flow past a model magnetosphere in the Ames Supersonic Free-Flight Wind Tunnel. Results are also presented that illustrate the distortion of the interplanetary magnetic field in the region between the bow and the magnetosphere for cases in which the magnetic field in the incident stream is inclined at 45° and 90° to the free-stream direction.

FACILITY FORM 602

N66-18351

(ACCESSION NUMBER)	74
(PAGES)	13
(NASA CR OR TMX OR AD NUMBER)	TMX 56548

(THRU)	1
(CODE)	13
(CATEGORY)	

Available to [redacted]
[redacted]

1. INTRODUCTION

Data obtained in space, particularly that from IMP-I (Explorer XVIII), have established beyond all doubt the existence of at least two classes of near discontinuities in plasma and magnetic field properties in the space surrounding the earth⁽¹⁾. One of these, the magnetopause, separates a region of rapidly flowing plasma with irregular magnetic fields from the magnetosphere where the magnetic field is considerably stronger and steadier and no plasma is detected by the plasma probes. Although it is presumed that plasma actually exists in the magnetosphere, the magnetopause marks the boundary of a region from which the rapidly streaming solar wind is excluded. Its shape conforms to that indicated by calculations based on the classical Chapman-Ferraro theory of the interaction of a dipole geomagnetic field and a fully ionized collisionless unmagnetized gas flowing radially outward from the sun. The second discontinuity is observed a few earth radii upstream of the magnetopause in a position that conforms remarkably well with the position of a bow shock wave in a supersonic flow past an obstacle having the shape of the magnetopause. Ness⁽²⁾ has also reported recently that data from the same satellite disclose the existence of a third discontinuity surface extending downstream from the earth inside the magnetosphere tail. In addition fluctuating magnetic fields were detected when the satellite was directly downstream from the moon, particularly on one occasion when IMP-I was near apogee at a geocentric distance of about 30 earth radii and approximately midway between the earth and moon^(3,4). This has been interpreted as the result of the satellite traversing the wake of the moon. These discoveries are

Available to NASA only

NASA Centers Only

of utmost importance to any discussion or analysis of the interaction between the solar wind and the geomagnetic field since they establish the general topology of the flow^(5,6).

These data strongly support the contention of Axford⁽⁷⁾, Kellogg⁽⁸⁾ and others that the collisionless interplanetary gas behaves like a continuum fluid on scales large compared with the gyroradius of a proton in the incident interplanetary field, i.e., about 500 km for representative conditions. The fact that the "discontinuities" are sometimes observed to be as thin as 100 km⁽⁹⁾ suggests that this may be a conservative estimate, and that the fluid model may be employed to discuss not only flow past the magnetosphere, but perhaps the smaller, and effectively unmagnetized, moon.

Although Ness, Scarce, and Seek⁽⁴⁾ and others have shown that theoretical results such as presented by Spreiter and Jones⁽¹⁰⁾ agree well with data from IMP-I, the logical foundations of the theory appear inconsistent. In particular, the magnetosphere boundary is computed by a simple modification of the Chapman-Ferraro theory, which is conventionally conceived as a particle model of the interaction, and the shock shape is calculated using continuum gasdynamic methods without any direct consideration of electromagnetic forces. With the concept adopted that large scale or time averaged features of the interaction between the solar wind and the geomagnetic field should be investigated in terms of a fluid theory, the simplest mathematical model capable of adequate description of many of the dominant features is provided by the equations of magnetohydrodynamics for a nondissipative perfect compressible gas. The appropriateness of this model for the present application involving flow of a collisionless

gas has been discussed recently by Lees⁽¹¹⁾, Levy, Petschek, and Siscoe⁽¹²⁾, and others, but it is not unfair to state that the principal justification derives from comparison of calculated and measured results and that a full theoretical justification does not exist at the present time. Perhaps the closest approach is that provided by the analysis of Chew, Goldberger, and Low⁽¹³⁾, but they do not find the pressure to be a scalar even when the transport of pressure along the magnetic field lines can be suppressed or ignored. It is possible that the pressure may nevertheless become a scalar as a result of instabilities or of small scale irregularities prevalent in the magnetic fields observed exterior to the magnetopause, but this is speculation at the present time. In spite of these uncertainties, the difficulties of solution of the nonlinear equations of magnetohydrodynamics and the richness of the phenomena contained within this theory are sufficiently great that it is worthwhile to explore the consequences of this model before introducing additional complications.

It is the purpose of this paper first to discuss the application of the fundamental equations and concepts of magnetohydrodynamics to the hypersonic flow of solar plasma around the earth and its magnetosphere, second to examine the degree to which the results may be approximated by the much simpler equations of gasdynamics, and third to present more extensive numerical results than have been available heretofore.

2. FUNDAMENTAL EQUATIONS

The fundamental differential equations of magnetohydrodynamics for the steady flow of a nondissipative (perfectly electrically conducting,

inviscid, nonheat conducting) perfect compressible gas are as follows (see, e.g., Landau and Lifshitz⁽¹⁴⁾),

$$\begin{aligned} \nabla \cdot \rho \underline{v} &= 0 \\ \rho(\underline{v} \cdot \nabla)\underline{v} + \nabla p &= -\frac{1}{4\pi} \underline{H} \times \underline{\text{curl}} \underline{H} = -\frac{1}{8\pi} \nabla H^2 + \frac{1}{4\pi} (\underline{H} \cdot \nabla)\underline{H} \\ \underline{\text{curl}}(\underline{H} \times \underline{v}) &= 0, \quad \text{div } \underline{H} = 0 \\ (\underline{v} \cdot \nabla)S &= 0, \quad p = e^{S/c_v \gamma} \end{aligned} \quad (1)$$

where ρ , p , S , and \underline{v} refer to the density, pressure, entropy, and velocity of the gas, \underline{H} refers to the magnetic field, $\gamma = c_p/c_v$, and c_p and c_v are constants representing the specific heats at constant pressure and constant volume. Important auxiliary relations for γ , temperature T , speed of sound a , internal energy e , and enthalpy h are as follow:

$$\begin{aligned} \gamma &= (N + 2)/N, \quad p = \rho RT/\mu = nkT \\ a &= (\partial p/\partial \rho)^{1/2} = (\gamma p/\rho)^{1/2} = (\gamma RT/\mu)^{1/2} \\ e &= c_v T, \quad h = c_p T = e + p/\rho \end{aligned} \quad (2)$$

where N represents the number of degrees of freedom, $R = (c_p - c_v)\mu = 8.314 \times 10^7 \text{ erg/}^\circ\text{K}$, $\mu = \text{mean molecular weight} = 1/2$ for fully ionized hydrogen plasma, $n = \text{number of particles/cm}^3 = 2n_p$ where n_p is the number of protons/cm³, and $k = \text{Boltzmann's constant} = 1.38 \times 10^{-16} \text{ erg/}^\circ\text{K}$. It is fully equivalent and convenient for some purposes to replace the entropy equation $(\underline{v} \cdot \nabla)S = 0$ in equation (1) by the following energy equation:

$$\text{div} \left[\rho \underline{v} \left(\frac{1}{2} v^2 + h \right) + \frac{\underline{v}}{4\pi} H^2 - \frac{1}{4\pi} (\underline{H} \cdot \underline{v})\underline{H} \right] = 0 \quad (3)$$

Although only first derivatives appear in equation (1), the fact that the neglected dissipative terms are described by second derivatives requires that the gradients be small. In magnetohydrodynamics, as in gas dynamics, however, compressions tend to coalesce and steepen into finite shock waves of such small thickness that they can be considered as virtual discontinuities for many purposes. In this way gradients tend to become very large, and continuous motions tend to break down some place if they involve compressions. In addition, attraction between like currents tends to cause current distributions to collapse into thin sheaths, across which the magnetic field can be considered in the same sense to be discontinuous. Mathematically, the solution of the dissipationless differential equations ceases to exist beyond the point of breakdown, and the flow is no longer governed solely by the relations given in equation (1). Mass, momentum, magnetic flux, and energy must still be conserved, however, and the following relations must hold between quantities on the two sides of any such discontinuity:

$$\begin{aligned}
 [\rho v_n] &= 0 \\
 \left[\rho v_n \gamma + \left(p + \frac{H^2}{8\pi} \right) \hat{n} - \frac{1}{4\pi} H_n \vec{H}_t \right] &= 0 \\
 \left[\rho v_n \gamma_t - \frac{1}{4\pi} H_n \vec{H}_t \right] &= 0, \quad [H_n] = 0 \\
 \left[\rho v_n \left(\frac{1}{2} v_n^2 + h \right) + v_n \frac{H^2}{4\pi} - \frac{1}{4\pi} H_n \gamma \cdot \vec{H} \right] &= 0
 \end{aligned} \tag{4}$$

The subscripts n and t refer to components normal and tangential to the discontinuity surface and $[Q] = Q_1 - Q_0$ where subscripts 0 and 1 refer

to conditions on the upstream and downstream sides of the discontinuity. These relations are frequently supplemented by the statement that there is a current sheet flowing along the discontinuity surface and that the value \underline{J}^* of this current per unit width is given by

$$\underline{J}^* = \underline{\text{curl}} \underline{H} \quad (5)$$

Friedrichs and Kranzer⁽¹⁵⁾ have developed an alternative form for the conservation equations that affords a quick survey of the possible types of discontinuities and some of their properties, and is particularly useful in the determination of asymptotic properties of weak discontinuities. It is based on extensive use of mean values $\langle Q \rangle = (Q_0 + Q_1)/2$, and the new variables $V = 1/\rho$ and $m = \rho v_n$ representing the specific volume and the mass flux across the discontinuity. In terms of these variables, the relations given in equation (4) are as follows:

$$\begin{aligned} m[V] - [v_n] &= 0 \\ m[y] + [p]\hat{n} + \frac{1}{4\pi} \langle \underline{H} \rangle \cdot [\underline{H}]\hat{n} - \frac{1}{4\pi} H_n[\underline{H}] &= 0 \\ m\langle V \rangle [\underline{H}] + \langle \underline{H} \rangle [v_n] - H_n[y] &= 0, \quad [H_n] = 0 \\ m \left\{ \left[e + \frac{VH^2}{8\pi} \right] + [V] \left(\langle p \rangle + \frac{1}{8\pi} \langle \underline{H}_t^2 \rangle - \frac{1}{8\pi} H_n^2 \right) - \frac{1}{4\pi} [V \underline{H}_t] \cdot \langle \underline{H}_t \rangle \right\} &= 0 \end{aligned} \quad (6)$$

The last of these may be replaced by

$$m \left\{ [e + \langle p \rangle V] + \frac{1}{16\pi} [V][\underline{H}_t]^2 \right\} = 0 \quad (7)$$

If the mean quantities are considered known, there are thus eight equations in eight scalar variables $[V]$, $[p]$, $[y]$, $[\underline{H}]$, and $[e]$; observe that $[H_n] = 0$ always.

Since e appears in only the last relation of equation (6), we can consider alternatively the seven scalar equations in seven variables defined by the first three relations of equation (6). They are all linear homogeneous equations, and solutions exist only if the determinant vanishes. Equating the determinant to zero yields the following equation for the mass flux m :

$$\langle V \rangle^2 m \left(\langle V \rangle m^2 - \frac{H_n^2}{4\pi} \right) \left\{ \langle V \rangle m^4 + \left(\frac{\langle V \rangle}{[V]} [p] - \frac{\langle H \rangle^2}{4\pi} \right) m^2 - \frac{[p] H_n^2}{[V] 4\pi} \right\} = 0 \quad (8)$$

With the density ρ_0 upstream of the discontinuity given, this equation can also be considered as an equation for the normal component of the incident velocity v_{n0} .

It may be seen immediately that $m = 0$ is a solution of equation (8), and that three additional plus-minus pairs of real roots exist for which $m \neq 0$. To follow Landau and Lifshitz⁽¹⁴⁾, we call discontinuities which lie along streamlines ($m = \rho v_n = 0$) tangential discontinuities or contact discontinuities according to whether or not the normal component of the magnetic field H_n vanishes. Discontinuities across which there is flow ($m \neq 0$) are divided into categories. Those associated with the roots $m = \pm H_n / (4\pi \langle V \rangle)^{1/2}$ are called rotational discontinuities, although they are frequently termed transverse or immediate shock waves by many authors. The term shock wave is reserved here, however, for the discontinuities associated with the four remaining roots.

3. TANGENTIAL DISCONTINUITIES

Tangential discontinuities are defined as those in which both m and H_n vanish. For these conditions, equations (4) and (6) yield the following relations between the quantities on the two sides of the discontinuity surface:

$$\begin{aligned} v_n = H_n = 0 ; \quad [v_t] \neq 0, \quad [H_t] \neq 0, \quad [\rho] \neq 0 \\ [p + H^2/8\pi] = [p^*] = 0 \end{aligned} \quad (9)$$

Although the velocity and magnetic field are required to be parallel to a tangential discontinuity, these relations show that the density and the tangential components of the velocity and magnetic field may have jumps of any magnitude. The other thermodynamic quantities, such as temperature, entropy, etc., are also discontinuous in accordance with their definitions provided in equation (2). The sum of fluid pressure p and magnetic pressure $H^2/8\pi$ must, however, be continuous across a tangential discontinuity.

It is important to observe that the properties of tangential discontinuities defined by equation (9) are compatible, although not identical, with those normally prescribed for the boundary of the geomagnetic field in the Chapman-Ferraro theory. In both cases, the condition $H_n = 0$ holds and requires that there is no connectivity between the geomagnetic field and the interplanetary field embedded in the solar wind. The differences stem from the additional assumptions in the Chapman-Ferraro theory that the incident plasma is free of magnetic field ($H_0 = 0$), and the cavity containing the geomagnetic field is free of plasma so that $p_1 = 0$; thus $p_0 = H_1^2/8\pi$. The absence of a magnetic field in the incident stream,

taken together with the extremely long mean free paths, implies there is no interaction between the particles prior to their encounter with the current sheath forming the boundary. The pressure is therefore taken to be proportional to the normal component of the momentum flux of the undisturbed incident stream, thus

$$K\rho_0 v_{n_0}^2 = K\rho_0 v_0^2 \cos^2 \psi = H_1^2 / 8\pi \quad (10)$$

where ψ is the angle between the normal to the boundary and the velocity vector of the undisturbed incident stream, and K is a constant equal to 2 if specular or "elastic" reflection is assumed, or unity if "inelastic" reflection is assumed.

4. CONTACT DISCONTINUITIES

The properties of contact discontinuities are given by solving equations (4) or (6) with $m = 0$ and $H_n \neq 0$. They are as follows:

$$v_n = 0, \quad H_n \neq 0; \quad [y] = [H] = [p] = 0, \quad [\rho] \neq 0 \quad (11)$$

These relations show that the fluid not only flows parallel to a contact discontinuity in a steady flow, but that the velocity, pressure, and magnetic field must be continuous. The density, and therefore the temperature, entropy, and other thermodynamic variables, may have any discontinuity, however.

The properties of contact discontinuities differ substantially from those used for the boundary of the geomagnetic field in the Chapman-Ferraro theory and from those observed in space over the forward part of the magnetopause by satellites such as IMP-I. They appear to be appropriate, however, for the boundary of the distant wake far downstream from the

earth or moon. There any current system or velocity discontinuity, such as exists on the forward part of the earth's magnetopause, has ample time to diffuse or decay no matter how slight the departures from perfect electrical conductivity or inviscid flow. Under these circumstances, the external magnetic field penetrates the discontinuity, and ultimately at great distances downstream may be expected to traverse the wake completely without distortion. Thermodynamic properties of the wake remain different from those of the surrounding flow, however, because of the different previous histories of the gases.

5. ROTATIONAL DISCONTINUITIES

The properties of rotational discontinuities are determined by solving equations (4) or (6) with $m = m_r = \pm H_n / (4\pi \langle v \rangle)^{1/2}$. They are

$$\begin{aligned} v_n &= \pm H_n / (4\pi \rho)^{1/2}, & [v_t] &= [H_t] / (4\pi \rho)^{1/2} \\ [\rho] &= [p] = [v_n] = [v^2] = [H^2] = 0 \end{aligned} \tag{12}$$

These relations show that the magnitudes of all quantities are continuous, and that the only changes across a rotational discontinuity are the directions of the magnetic field and velocity vectors, both of which rotate by an equal angle about the normal to the discontinuity. The flow velocity component v_n normal to a rotational discontinuity is equal to the phase velocity of an Alfvén wave in the direction of the wave normal, and is moreover independent of the strength of the discontinuity. There is thus no tendency for a series of weak rotational discontinuities in a homogeneous medium either to overtake one another and coalesce into a shock wave or to spread out as in an expansion fan. Although there has been considerable

discussion of possible effects of traveling rotational or Alfvén waves in the magnetosphere and in space (see, e.g., MacDonald⁽¹⁶⁾ for a recent review), the role and importance of stationary rotational discontinuities in the steady state flow of solar plasma past the earth or moon are not known.

6. SHOCK WAVES

The mass flux m through magnetohydrodynamic shock waves satisfies the equation

$$\langle v \rangle m^4 + (\langle v \rangle [p]/[V] - \langle H \rangle^2 / 4\pi) m^2 - [p] H_n^2 / 4\pi [V] = 0 \quad (13)$$

obtained by setting to zero the last factor of equation (8). Equation (6) together with the further requirement stemming from entropy considerations that all shock waves are compression waves yields the following relations between the quantities on the two sides of such a shock wave

$$\begin{aligned} [H_t] = [H] &= \frac{-m^2 [V] \langle H_t \rangle}{\langle v \rangle m^2 - H_n^2 / 4\pi}, & [H_n] &= 0, & [H]^2 &= 2 \langle H \rangle \cdot [H] \\ [v_t] &= - \frac{m [V] H_n \langle H_t \rangle / 4\pi}{\langle v \rangle m^2 - H_n^2 / 4\pi}, & [v_n] &= -[V] m, & [V] < 0, & [p] > 0 \end{aligned} \quad (14)$$

where m represents any of the four roots of equation (13). The first of these indicates that the sum $2 \langle H_t \rangle$ and difference $[H_t]$ of the tangential components of the magnetic fields on the two sides of the shock wave lie in either the same or opposite directions. This requires the shock normal \hat{n} and the magnetic field vectors on the two sides of the

discontinuity to be coplanar. The velocity relations also show that the tangential component of the velocity discontinuity $[y_t] = y_{t_1} - y_{t_0}$ is in the same or opposite direction as $\langle H_t \rangle$ and therefore in the same plane as H_0 and H_1 .

Discussion of the properties of shock waves characterized by the various roots for m is facilitated by rewriting equation (13) as follows:

$$(m^2 + [p]/[V])(\langle V \rangle m^2 - H_n^2/4\pi) = m^2 \langle H_t \rangle^2 / 4\pi \quad (15)$$

Since the roots $m = m_r = \pm H_n / (4\pi \langle V \rangle)^{1/2}$ are not considered in this section, it follows that $m_F^2 > -[p]/[V]$ if $m^2 = m_F^2 > m_r^2$, and conversely that $m_S^2 < -[p]/[V]$ if $m^2 = m_S^2 < m_r^2$. Shock waves characterized by the larger value m_F for the mass flux are called fast, those by the smaller value m_S slow. The mass flux across either class of shock waves must therefore satisfy the inequalities

$$m_F \geq m_r \geq m_S, \quad m_F \geq -[p]/[V] \geq m_S \quad (16)$$

It follows immediately from equations (14) and (16) that H_t , H^2 , and y_t all increase through a fast shock wave, and decrease through a slow shock wave.

Solutions of equations (4) or (6) are determined by straightforward but lengthy algebraic manipulation, details of which are available in several sources (see, e.g., Anderson⁽¹⁷⁾ or Jeffrey and Taniuti⁽¹⁸⁾ for recent summaries). It is important to recognize, however, that these equations possess extraneous solutions that cannot occur in nature. These solutions were originally referred to as unstable, but this term has now been generally abandoned as it has become known that this is not an ordinary instability growing exponentially with time, but rather a sudden

disintegration of the shock wave. Alternatively, a solution containing an extraneous shock wave does not have neighboring solutions corresponding to a small change in the boundary condition which requires an arbitrarily small angle of rotation of the plane of the magnetic field. Identification of the physically relevant solutions cannot be made on the basis of entropy considerations alone, as in ordinary gasdynamics. It is necessary in magnetohydrodynamics to consider how a shock wave could evolve through waves of small amplitude overtaking one another and coalescing. The appropriate requirements for a physically relevant solution may be stated in general mathematical terms by a pair of evolutionary conditions (see, e.g., Jeffrey and Taniuti⁽¹⁸⁾). A more physical description that leads to the same conclusions has been given recently by Kantrowitz and Petschek⁽¹⁹⁾. From either point of view, it is found that no additional conditions need be imposed for fast shock waves, and that the conservation equations possess extraneous solutions only for slow shock waves. Fortunately, the extraneous solutions can be recognized easily by the fact that they indicate the tangential component of the magnetic field to be directed oppositely on the two sides of the discontinuity, a physical impossibility in all but certain degenerate cases. Since the first of equations (14) shows that the tangential component of the magnetic field cannot reverse direction through a fast shock wave, one has the general result that the tangential components of the magnetic field on the two sides of any physically relevant shock wave must always lie in the same direction. A further consequence of these considerations is that the flow velocity must be greater than the rotational wave speed on both sides of a fast shock wave, and less than the rotational wave speed on both sides

of a slow shock wave. It follows immediately that a fast shock wave overtakes a slow shock wave, and that a slow shock wave cannot overtake a fast shock wave. In application to the supersonic flow of the solar wind past either the earth's magnetosphere or the solid moon, it is anticipated therefore that the bow wave would be a fast magnetohydrodynamic shock wave. Slow shock waves, as well as additional fast shock waves, may be expected in the flow downstream of the bow wave, however.

7. WEAK SHOCK WAVES

The relations given in equations (13) and (14) simplify for weak shock waves to the point where they can be expressed explicitly in terms of the sound speed a , the Alfvén speed A , and its components A_n and A_t normal and tangential to the plane of the discontinuity surface. The latter are defined as follows:

$$A = (H^2/4\pi\rho)^{1/2}, \quad A_n = (H_n^2/4\pi\rho)^{1/2} = A|\cos \theta|, \quad A_t = (H_t^2/4\pi\rho)^{1/2} = A|\sin \theta| \quad (17)$$

where θ refers to the angle between the magnetic field \underline{H} and the shock normal \hat{n} . For such shock waves, the jump $[Q]$ in every quantity Q is much smaller than the quantity itself, and the desired simplification can be accomplished by simply removing the mean value brackets and replacing, for clarity of expression, the difference brackets with δ , i.e., $\langle Q \rangle = Q$, $[Q] = \delta Q$. Equation (13) may then be solved to yield the following expression for the normal velocity component v_n of the incident stream:

$$v_n = \pm \left[\frac{1}{2} \left\{ a^2 + A^2 \pm \sqrt{(a^2 + A^2)^2 - 4a^2A_n^2} \right\} \right]^{1/2} \quad (18)$$

With v_n taken positive, the larger of the two values obtained by using the plus sign before the inner radical pertains to the fast wave, and the smaller to the slow wave.

Equation (18) coincides with the corresponding expression for the velocity component normal to the characteristic surfaces of equation (1), and may be recognized, upon changing to a reference frame fixed in the fluid upstream of the shock wave, as the appropriate expression for the phase velocities of fast and slow traveling hydromagnetic plane waves. The propagation of such waves is conveniently described graphically by the familiar normal speed or Friedrichs I diagrams, examples of which are shown in Fig. 1 for $a = \sqrt{2}A$, $a = A$, and $a = A/\sqrt{2}$. In these diagrams, v_n is plotted as a function of angle θ between the shock normal and the magnetic field \underline{H} (here taken parallel the horizontal axis). The outer curve in each diagram represents the results for the fast wave, the inner curves the results for the slow wave. Also included are dotted curves representing the normal velocity of a rotational discontinuity defined by equation (12). For ease of illustration, the diagrams are drawn for the plane containing the wave normal and the magnetic field vectors. The corresponding results for more general orientations are represented by the corresponding three-dimensional surfaces formed by rotating the plane curves of Fig. 1 about the $\theta = 0$ axis. These plots illustrate that, for any direction θ , the speed of a rotational wave is intermediate between that of the fast and slow waves. Further, v_n for the fast wave is equal to the larger of a and A when the wave normal is parallel to \underline{H} ($\theta = 0$), and to $(a^2 + A^2)^{1/2}$ when the wave normal is perpendicular to \underline{H} ($\theta = \pi/2$). For the slow wave, v_n vanishes when $\theta = \pi/2$, and is equal to the smaller

of a and A when $\theta = 0$. If A approaches zero while a remains finite, the surfaces representing the slow and rotational waves disappear and the surface representing the fast wave approaches a sphere of radius a . Under these circumstances, the equations of magnetohydrodynamics approach those of gasdynamics, and calculations based on aerodynamic methods should provide a good approximation for most applications. If, on the other hand, a approaches zero while A remains finite, the surfaces representing the slow wave disappear, that representing the fast wave approaches a sphere of radius A , and those representing the rotational discontinuity are spheres of radius $A/2$ as always. Although equation (18) clearly shows the normal velocity of fast and slow waves to be invariant with interchange of values for a and A , and the former to become independent of direction θ as a vanishes, it is important to observe that rotational discontinuities retain a finite normal velocity and that neither the differential equations nor shock relations of magnetohydrodynamics approach those of gasdynamics in this limit (except in a special and restricted sense for flows in which the velocity and magnetic field vectors are parallel at all points⁽¹⁹⁾).

The jump relations given in equation (14) reduce similarly in the limit of weak shock waves to

$$\delta H_t = \frac{v_n^2 H_t}{v_n^2 - A_n^2} \frac{\delta \rho}{\rho}, \quad \delta H_n = 0, \quad \delta H^2 = 2H \cdot \delta H \quad (19)$$

$$\delta v_t = \left(\frac{v_n A_t A_n}{v_n^2 - A_n^2} \right) \frac{\delta \rho}{\rho} \left[\frac{H_t H_n}{|H_t| |H_n|} \right], \quad \delta v_n = v_n \delta \rho$$

where the quantity in the last bracket of the expression for δv_t gives

the direction and sign of that quantity. The corresponding expressions for the change in pressure p and entropy S across a weak shock wave are (see, e.g., Jeffrey and Taniuti⁽¹⁸⁾)

$$\frac{\delta p}{p} = \gamma \frac{\delta \rho}{\rho} + \frac{\gamma(\gamma - 1)}{2} \left(\frac{\delta \rho}{\rho}\right)^2 + \left\{ \frac{\gamma(\gamma - 1)^2}{4} + \frac{\gamma(\gamma - 1)v_n^4}{4(a^2/A_t^2)(v_n^2 - A_n^2)^2} \right\} \left(\frac{\delta \rho}{\rho}\right)^3 + \dots \quad (20)$$

$$\delta S = c_v \frac{\gamma(\gamma - 1)}{4} \left\{ \frac{\gamma + 1}{3} + \frac{v_n^4}{(v_n^2 - A_n^2)^2(a^2/A_t^2)} \right\} \left(\frac{\delta \rho}{\rho}\right)^3 + \dots$$

The latter relation shows the change in entropy through a weak shock wave to be proportional to only the third power of $\delta\rho/\rho$, and hence to be vanishingly small for weak waves. Physically, this indicates that infinitesimal expansions, as well as compressions, may be considered without violation of the entropy requirement. Thus $\delta\rho$ may be either positive or negative. Moreover, equation (20) shows that, although the change in pressure through a weak discontinuity is proportional to $\delta\rho/\rho$, the first term in which the magnetic field appears is proportional to $(\delta\rho/\rho)^3$. The changes in entropy and pressure through magnetohydrodynamic expansions or compressions are thus the same as in gasdynamics until the strength of the discontinuity is sufficiently great that third order terms must be retained. As indicated by equation (19), however, this statement does not extend to other quantities such as the velocity or the magnetic field.

These results for weak compression and expansion waves are useful for describing conditions at great distances from the earth or other disturbing obstacles where it can be safely assumed that $\delta\rho/\rho \ll 1$. They are not sufficient for the discussion of the entire bow wave problem, however, because conditions typical of the solar wind in the vicinity of the

earth's orbit are such that $\delta\rho/\rho$ may easily exceed unity near the nose. The maximum value for the density ratio across a hydromagnetic shock wave is finite, however, and given simply by $\rho_1/\rho_0 = (\gamma + 1)/(\gamma - 1)$, just as in gasdynamics.

8. GEOPHYSICAL APPLICATION

The concepts and equations of magnetohydrodynamics summarized in the preceding sections will now be applied to the specific geophysical problem of the interaction of a steady solar wind and the geomagnetic field. The permanent component \underline{H}_p of the latter is represented by a centered magnetic dipole having a magnetic moment $M_p = H_{p0}a_e^3$, where $H_{p0} = 0.312$ gauss represents the earth's mean permanent field at the geomagnetic equator and $a_e = 6.37 \times 10^8$ cm represents the mean radius of the earth. With the dipole located at the origin and aligned with the coordinate system as illustrated in Fig. 2, \underline{H}_p is given by

$$\underline{H}_p = -(M_p/r^3)(\hat{\theta} \sin \theta + \hat{r} \cos \theta) \quad (21)$$

The total magnetic field at any point is then the sum of \underline{H}_p and the induced magnetic field \underline{H}' due to currents in the plasma.

Two important parameters that characterize the flow at any point are the Mach number M and the Alfvén Mach number M_A defined by

$$M = v/a, \quad M_A = v/A \quad (22)$$

where a represents the speed of sound defined in equation (2), A the speed of an Alfvén wave defined in equation (17), and $v = |\mathbf{y}|$ represents the fluid speed. Values for a and A for conditions typical of those encountered in the solar wind as it flows around the magnetosphere are illustrated in Fig. 3. The solar wind is known to vary substantially with time, but number densities of the order of 2.5 to 25 protons/cm³, magnetic fields of 3 to 10 γ ($1\gamma = 10^{-5}$ gauss), and temperatures of 50,000 to 100,000^oK may be considered representative. Since the velocity of the incident solar wind ranges from about 300 to 800 km/sec, it is evident that the free-stream Mach number M_{∞} and Alfvén Mach number $M_{A_{\infty}}$ are generally much greater than unity.

(a) Asymptotic directions of shock waves and wake

When M_{∞} and $M_{A_{\infty}}$ are given together with the directions of the velocity and magnetic field vectors \mathbf{v}_{∞} and \mathbf{H}_{∞} in the undisturbed incident solar wind, the asymptotic directions of the magnetosphere tail (or wake) and shock waves at great distances from an obstacle can be determined immediately by a simple geometrical construction based on the normal speed diagrams of Fig. 1. The results apply equally whether the obstacle is in effect the confined magnetic field as in the case of the earth's magnetosphere, or the solid object itself if its magnetic field is not sufficiently strong to withhold the solar wind. Although their

magnetic fields have not yet been determined with sufficient accuracy to make a definitive statement, the moon and Venus may be examples of the latter possibility.

This construction is illustrated in Fig. 4(a) for a case in which the magnetic field vector \underline{H}_∞ is inclined 45° from the free-stream velocity vector, and $M_A = \sqrt{2}M$. For ease of illustration, M_∞ has been assigned a somewhat low value of 2, and only the traces of the various three-dimensional surfaces in the plane containing the velocity and field vectors are shown. The origin is placed in the obstacle, and the horizontal axis is aligned with the direction of the free-stream velocity vector \underline{v}_∞ as indicated. With center at the tip of the vector \underline{v}_∞ , and θ measured from the direction of \underline{H}_∞ , equation (18) is used to construct curves representing the normal velocities of weak shock waves and rotational discontinuities. Except for a translation of the origin and rotation of the axis, the latter are, of course, the same as shown in Fig. 1 for $a/A = \sqrt{2}$. The asymptotic directions of the various discontinuities at great distances from the obstacle can now be determined by application of the theorem that states that the two lines drawn from any point on a circle to the extremities of a diameter intersect at a right angle. The required construction is thus performed simply by drawing a circle of radius $v_\infty/2$ with center at $\underline{v}_\infty/2$ and connecting the origin to the various points of intersection with the

normal speed curves by straight lines as indicated in Fig. 4(a). The asymptotic directions can also be determined by constructing tangents to the related Friedrichs II diagram for the waves from a point disturbance as described by Sears⁽²¹⁾ and illustrated in Fig. 4(b), but the construction employed in Fig. 4(a) is more direct and fully equivalent for the present purposes.

Also indicated in Fig. 4 is the asymptotic direction of the magnetosphere tail or wake, which as noted previously would be represented by either a tangential discontinuity or a contact discontinuity depending upon whether the normal component of the magnetic field vanishes or not. In either case, equations (9) and (11) show that $v_n = 0$ indicating that the wake must be aligned parallel to \underline{v}_∞ independently of the direction of the magnetic field. The orientations of the other discontinuities illustrated in Fig. 4 change, however, as the direction of the magnetic field vector is altered. The extent of these changes can be readily visualized, moreover, since a change in the direction of the magnetic field leads to a rotation of the Friedrichs speed diagrams about the end of the fixed \underline{v}_∞ vector, and this in turn leads to associated changes in the intersection points of Fig. 4(a) or the tangency points of Fig. 4(b).

(b) Relation between hydromagnetic and gasdynamic flows

Although the diagrams of Fig. 4 are for the case in which the free-stream Mach number is 2 and the speed of sound is $\sqrt{2}$ times the Alfvén speed, that is for $(a/A)_{\infty} = (4\pi\gamma p_{\infty}/H_{\infty}^2)^{1/2} = \sqrt{2}$, the qualitative character of these diagrams remains the same for all Mach numbers and ratios $(a/A)_{\infty}$ greater than unity. If A_{∞} should become small relative to a_{∞} , however, as might readily occur if the magnetic field should diminish in intensity, the inner loops representing the propagation speeds of rotational and slow waves become small relative to the outer ovals representing the fast waves. Finally, if the magnetic field approaches zero, the inner loops shrink toward a point at the end of the x_{∞} vector while the outer oval approaches a circle (or sphere in the corresponding three-dimensional representation) of radius a_{∞} . In this way, the fast hydro-magnetic wave degenerates to the Mach wave of ordinary gasdynamics, and the rotational and fast waves lose their physical significance. The fluid and electromagnetic aspects of the flow thus decouple, and the fluid motion is described entirely by the equations of gasdynamics. The approach to the limiting case appears, moreover, to be free of singular behavior and it is to be expected that gasdynamic theory will provide a useful approximation to hydromagnetic flows when $(a/A)_{\infty}$ is substantially greater than unity. It should be observed, however, that the gasdynamic Mach number should be associated with the Mach number M of the corresponding hydro-magnetic flow, rather than the Alfvén Mach number M_A as has been done in most previous discussions of this application.

If, on the other hand, the Alfvén speed is substantially greater than the sound speed, as would occur if the magnetic field is sufficiently strong, the inner loops representing the slow wave speed again shrink toward a point at the end of the v_∞ vector, while the outer oval representing the fast wave speed approaches a circle of radius A_∞ . The resulting asymptotic directions for fast waves in a hydromagnetic flow of Alfvén Mach number M_{A_∞} thus approach those of gasdynamics for Mach number $M_\infty = M_{A_\infty}$. As described by Sears⁽²¹⁾ and others, the flows are not necessarily similar, however, because the physically significant waves for certain combinations of M_∞ , M_{A_∞} , and angles between v_∞ and H_∞ are those that extend upstream rather than downstream from the disturbance. When such conditions prevail, hydromagnetic flow about a given obstacle may still tend to resemble gasdynamic flow about the same obstacle, but the flow direction of the related incident stream must be reversed.

(c) Aligned flows

Clarification of the latter point can be attained by considering the case in which the magnetic field is aligned with the velocity vector in a steady and uniform incident stream. Imai⁽²⁰⁾, Grad⁽²²⁾, and others have shown for this case that the differential equations and conservation relations of hydromagnetic flow (i.e., equations (1) and (4)) require that

$$\mathbb{H} = \lambda \rho v \quad (23)$$

where λ is constant on a streamline. More importantly, they have also shown that these equations can be reduced to those of conventional gasdynamics (although of a hypothetical gas having an unusual equation of

state) upon introduction of the pseudoquantities related to the actual physical quantities as follows:

$$\begin{aligned}
 y^* &= y[1 - (\lambda^2 \rho / 4\pi)] = y(1 - M_A^{-2}) \\
 \rho^* &= \rho[1 - (\lambda^2 \rho / 4\pi)]^{-1} = \rho(1 - M_A^{-2})^{-1} \\
 p^* &= p + H^2 / 8\pi \\
 S^* &= S
 \end{aligned}
 \tag{24}$$

The equation of state of the hypothetical gas is given by

$$p^*(\rho^*; S, \lambda, h_0) = p(\rho, S) + \lambda^2 \rho^2 [h_0 - h(\rho, S)] / 4\pi \tag{25}$$

Application of the thermodynamic relations $dh = dp/\rho$ and $a^2 = \partial p / \partial \rho$ along a streamline yields the following important auxiliary relations

$$\begin{aligned}
 h^* &= h + A^2(1 - M_A^{-2}/2) \\
 a^* &= (1 - M_A^{-2})^2 [a^2(1 - M_A^{-2}) + A^2] \\
 M^{*2} &= (v^*/a^*)^2 = M^2 M_A^2 / (M^2 + M_A^2 - 1)
 \end{aligned}
 \tag{26}$$

where h_0 is the stagnation enthalpy on a given streamline. The approach to gasdynamics as H tends to zero and M_A to infinity is clearly evident from these relations. Although the mathematical analog holds for all M_A , it is clearly inconvenient for M_A less than unity since the pseudodensity ρ^* is negative, and the analog flow is in the reverse direction to the actual flow since y^* and y are of opposite sign. Nevertheless, such applications have been carried out in complete detail for sub-Alfvénic ($M_A < 1$) flow past an obstacle (see, e.g., Tamada⁽²³⁾).

To complete the analog, consider the way in which the boundary conditions transform when the relations of equation (24) are applied. With M_A typically substantially greater than unity in the free stream, the boundary

condition of uniform flow of given M_∞ and M_{A_∞} at great distances from the obstacle transforms directly into a uniform flow in the same direction having a pseudo Mach number $M_\infty^* = M_\infty M_{A_\infty} / (M_\infty^2 + M_{A_\infty}^2 - 1)^{1/2}$. In applications to hydromagnetic flow around an unmagnetized planet or moon, the boundary condition that $v_n = 0$ at the body surface carries over unchanged as $v_n^* = 0$, and the entire problem reduces immediately to a standard, although nonlinear and difficult, problem in gasdynamics.

Additional considerations are necessary, however, in applications to flow around the magnetosphere of a magnetized planet such as the earth for which the location of the tangential discontinuity representing the magnetosphere boundary must be determined as part of the solution. The condition specified in equation (23) is satisfied everywhere outside the magnetosphere boundary whenever \underline{H}_∞ and \underline{v}_∞ are parallel, but extension of this condition to the interior of the magnetosphere appears neither necessary nor appropriate. To be more explicit, all estimates of the magnitudes of the gas pressure p and the magnetic pressure $H^2/8\pi$ in the outer magnetosphere lead to the conclusion that $p \ll H^2/8\pi$. So far as the flow outside the magnetosphere is concerned, the magnetosphere boundary may thus be represented by the limiting case of a tangential discontinuity in which there is a vacuum ($\rho = 0$) on one side, and across which the sum of gas and magnetic pressure of the exterior flow must be balanced entirely by the magnetic pressure of the magnetosphere. The magnetosphere boundary thus becomes a real boundary of the flow and the analog to gasdynamics is completed except that the shape and size of the obstacle corresponding to the magnetosphere is not known a priori, but must be determined as part of the solution much as in the classical theory of

free-streamline flows in hydrodynamics (see, e.g., Lamb⁽²⁴⁾). The form and size of the magnetosphere boundary are, however, effectively independent of the details of flow within the magnetosphere, and determined primarily by the interaction between the magnetic field within the magnetosphere and the hydromagnetic flow around the exterior. There is still flow to be expected within the magnetosphere, but it would be required to move about as if it were confined in a container described by the magnetosphere boundary.

9. RESULTS OF GASDYNAMIC CALCULATIONS

Although the experimental confirmation by IMP-I satellite of the theoretical location of the magnetosphere boundary and associated bow shock wave calculated by Spreiter and Jones⁽¹⁰⁾ provides one of the major justifications for the study of continuum models for the flow of solar plasma around the magnetosphere, it should be observed that these calculations are accomplished through use of four important approximations, the accuracies of which are not immediately self-evident. First, the flow around the magnetosphere and the position of the shock wave are calculated by means of gasdynamic rather than hydromagnetic theory. Second, the fluid pressure at each point of the magnetosphere boundary is assumed to be given by the simple Newtonian formula $K\rho_{\infty}v_{\infty}^2 \cos^2 \psi$ where in contrast to the notation used in equation (10) the density and velocity of the undisturbed incident stream are represented by ρ_{∞} and v_{∞} , and K is a constant equal to unity. Third, the magnetic field just inside the magnetosphere boundary which provides the balancing magnetic pressure $H^2/8\pi$ is assumed to be approximated sufficiently well by twice the

tangential component of the geomagnetic dipole field. Fourth, the shape of the magnetosphere boundary is approximated by an axisymmetric figure defined by rotating about the sun-earth line the equatorial plane trace of the magnetosphere boundary calculated with the second and third approximations.

Except for the special case of aligned flow for which Imai's analog defined by equations (23) through (26) can be applied, the first approximation is virtually a necessity at the present stage of capabilities in the solution of supersonic flow around blunt obstacles, but fortunately is probably justifiable in most cases on the basis of the high Alfvén Mach number characteristic of the flow at all points outside the magnetosphere.

The second may appear to be a vestigial remnant of the older free particle model of Chapman and Ferraro (see, e.g., Chapman⁽²⁵⁾ for a review) for the magnetosphere boundary, but will be shown herein to actually provide a good approximation for the pressure in the fluid model, particularly if a slight adjustment is made in the value of the coefficient K . Its use has the very important effect of enabling the shape of the magnetosphere boundary to be determined without further consideration of details of the surrounding flow.

The third approximation is purely a convenience at this stage of the analysis. The shape of the complete magnetosphere boundary has been determined by using this approximation by Briggs and Spreiter⁽²⁶⁾ and without it, but with the pressure still given by the Newtonian formula by Midgeley and Davis⁽²⁷⁾ and Mead and Beard⁽²⁸⁾. As shown by

the latter authors, however, the exact and approximate coordinates of the boundary differ by only a few per cent. In any case, further simplification of the shape of the magnetosphere boundary is necessary since the present state of development of the theory of supersonic flow around three-dimensional blunt nose obstacles enables calculations to be made only for axisymmetric flows, and the magnetosphere boundary is not indicated to be perfectly axisymmetric by any of the above calculations.

The principal gasdynamic result presented by Spreiter and Jones⁽¹⁰⁾ was a plot of the calculated position of the bow shock wave associated with the simplified axisymmetric magnetosphere described in the preceding paragraphs. The calculations were performed for a ratio of specific heats γ of 2, and a free-stream Mach number of 8.71. The latter was identified with the free-stream Alfvén Mach number associated with a representative choice of values for the density, velocity, and magnetic field of the incident solar wind. It follows from the discussion of the preceding sections, however, that the gasdynamic Mach number should more properly be identified either with the free-stream pseudo Mach number M^* defined in equation (26) if the flow is aligned with the magnetic field and the Alfvén Mach number is greater than unity, or with the free-stream Mach number if the field has arbitrary alignment and is sufficiently weak that the Alfvén Mach number is much greater than unity. Further results of the gasdynamic calculations were not presented, however. It is therefore the first purpose of this section to provide further details of the flow field, such as, the density, velocity, temperature, etc. In order to facilitate comparison and interpolation, these results are presented for a free-stream Mach number of 8 rather than 8.71.

The necessary calculations have been carried out by the same methods employed by Spreiter and Jones⁽¹⁰⁾; namely those described by Inouye and Lomax⁽²⁹⁾ using the basic method of Van Dyke⁽³⁰⁾ and Van Dyke and Gordon⁽³¹⁾ as modified by Fuller⁽³²⁾. The method used for the subsonic region and the immediately adjoining portion of the supersonic region is an indirect one in which the location of the bow shock wave and the conditions across it are given and the resulting flow field and body shape are found as part of the solution. The solution for the desired body, the magnetosphere boundary in the present application, is then found by iteration following judicious selection of the trial bow shock wave shape based on experience with a vast number of cases of aerodynamic interest. A more complete discussion of details of the method including related mathematical aspects, such as, convergence, stability, and accuracy, has recently been given by Lomax and Inouye⁽³³⁾. The solution for the remainder of the supersonic region is accomplished by the method of characteristics described explicitly by Inouye and Lomax⁽²⁹⁾.

Figure 5 shows a plot of the magnetosphere boundary and shock wave position for $\gamma = 2$ and $M_\infty = 8$ in terms of a dimensionless length scale in which the distance D from the center of the earth to the magnetosphere nose is unity. The appropriate expression for D consistent with the assumptions enumerated at the beginning of this section is

$$D = a_e H_{p_0}^{1/3} / (2\pi K \rho_\infty v_\infty^2)^{1/6} \quad (27)$$

where $a_e = 6.37 \times 10^8$ cm and $H_{p_0} = 0.312$ gauss as noted previously. It is now well established that D is generally of the order of 10 earth radii, and fluctuates with time in response to variations in the density

ρ_∞ and velocity v_∞ of the incident stream. Except for the normalization of the distance scale and slight changes due to the difference in free-stream Mach number, the curves shown in Fig. 5 are exactly as given by Spreiter and Jones⁽¹⁰⁾. Also included on this figure, however, are several additional solid lines representing streamlines, and broken lines representing characteristic or Mach lines of the flow. The latter correspond to standing compression or expansion waves of infinitesimal amplitude. As indicated by equation (18) with $A = 0$, they cross the streamlines at such angles that the local velocity component normal to the wave is always exactly equal to the local sound speed. Mach lines thus exist only where the flow is supersonic; their absence from the vicinity of the magnetosphere nose is a consequence of the flow there being subsonic. This plot also shows that the angle between the shock wave and the incident stream is much larger than the asymptotic angle along the entire length of the shock wave included in the illustration, the asymptotic angle being easily recognized as equal to the angle between the streamlines and Mach lines of the incident undisturbed flow upstream from the bow shock wave. It follows at once that knowledge of the asymptotic directions of weak shock waves is of limited usefulness in the estimation of the location of the bow shock wave, except at extremely great distances from the earth.

Contour maps showing lines of constant density ρ , velocity v , temperature T , and mass flux ρv , each normalized by dividing by the corresponding quantity in the incident stream, are presented in Figs. 6, 7, and 8 for the same conditions as in Fig. 5, namely, $M_\infty = 8$ and $\gamma = 2$.

It can be seen that the density ratio ρ/ρ_∞ immediately behind the shock remains close to the maximum value $(\gamma + 1)/(\gamma - 1) = 3$ for a strong shock wave in a gas with $\gamma = 2$ along nearly the entire length of the bow wave shown. The gas undergoes only a small additional compression as it nears the stagnation point at the magnetosphere nose and then expands to less than free-stream density as it flows around the magnetosphere. The velocity remains less than in the free stream, however, throughout the same region. The temperature ratio T/T_∞ is closely related to the velocity ratio through the expression

$$\frac{T}{T_\infty} = 1 + \frac{(\gamma - 1)M_\infty^2}{\gamma} \left(1 - \frac{v^2}{v_\infty^2}\right) \quad (28)$$

derived by integrating equation (3) with $\underline{H} = 0$, combining with relations for the enthalpy h and speed of sound a given in equation (2), and rearranging. If values for γ and M_∞ are given, it is then a straightforward and simple calculation to determine T/T_∞ as a function of v/v_∞ . The results presented in Fig. 7 show that the temperature is substantially higher than in the free stream throughout the entire region illustrated in Figs. 5 through 8. If, e.g., the temperature of the incident solar wind is $50,000^\circ\text{K}$, the temperature at the magnetosphere nose is indicated to be nearly $2,000,000^\circ\text{K}$. This value is consistent with the temperature possessed by the gas in the solar corona before it was accelerated to the high velocities characteristic of the solar wind in the vicinity of the earth's orbit. Although the gas cools considerably as it flows around the magnetosphere, it is still about $850,000^\circ\text{K}$ as it passes the station of the earth ($x/D = 0$) and about $400,000^\circ\text{K}$ farther downstream at $x/D = 1$.

Although the mass flux ratio is simply the product of ρ/ρ_∞ and v/v_∞ already illustrated in Figs. 6 and 7, it is included here because of its relation to the quantity customarily measured by plasma probes and because of the interesting shapes of the contours. It should be observed before closing this discussion that the constant velocity contours of Fig. 7 can also be used to represent, with a suitable relabeling, lines of constant local Mach number $M = v/a$. This statement follows from equations (2) and (28) which show that a is proportional to $T^{1/2}$ for a given pair of values for γ and μ , and T/T_∞ depends only on v/v_∞ for given M_∞ and γ . There exists, therefore, for flow characterized by given M_∞ , γ , and μ , a unique value for M associated with every value for v/v_∞ . Contours for constant local Mach number are thus identical to those for constant velocity ratio. Similarly, since the mean velocity of the particles is proportional, but not equal, to the speed of sound according to the simple kinetic theory of a gas, contours of constant ratio of directed to random velocity are also identical to those for constant v/v_∞ .

The choice of the value 2 for the ratio of specific heats employed in calculating Figs. 5 through 8 is justified in a variety of ways, generally centering around the presumed two-degree-of-freedom nature of the interactions of charged particles in a magnetic field. This argument weakens, however, when consideration is given to the extremely irregular character of the magnetic fields observed in space, particularly downstream of the bow shock wave. In fact, the whole concept of applying hydromagnetic theory to the flow of solar plasma around the magnetosphere involving as it does the assumption of an isotropic pressure appears more

consistent internally if the particles are considered to behave as if they have three rather than two degrees of freedom. Since $\gamma = (N+2)/N$ where N is the number of degrees of freedom, results parallel to those presented in Figs. 5 through 8 have been calculated for $M_\infty = 8$ and $\gamma = 5/3$. The results, presented in Figs. 9 through 12, are similar in all qualitative features to those for $\gamma = 2$. Quantitatively, however, the standoff distance of the shock wave is less, the density is generally somewhat higher, and the temperature substantially lower for $\gamma = 5/3$ than for $\gamma = 2$.

Reference to Fig. 3 and the accompanying discussion shows that the value of 8 for the free-stream Mach number is well centered in the range of values to be expected in the incident solar wind. The velocity and temperature, and therefore the speed of sound, vary over a considerable range, however, and it is of interest to determine the extent to which conditions in the flow around the magnetosphere change with Mach number. Further calculations have been made therefore for Mach numbers of 5 and 12 for a gas with $\gamma = 5/3$. Since most of the results are so similar to those presented above, they are presented in abridged form in Figs. 13 through 15. Figure 13 shows the position of the bow shock waves for these conditions together with the results for $M_\infty = 8$, shown in Figs. 5 and 9. It can be seen that the bow wave recedes from the magnetosphere as the Mach number diminishes and as γ increases. The change is small, however, as the Mach number is increased from 8 to 12. The entire portion of the bow wave shown in these figures is, in fact, very near its asymptotic position for infinite Mach number, and further increases in Mach

number are virtually without effect. This lack of dependence on Mach number does not apply, however, far downstream of the earth where the bow wave approaches alignment with the asymptotic direction of weak discontinuities in the undisturbed incident solar wind. The variation of density, velocity, and mass flux along the magnetosphere boundary and the downstream side of the shock wave are shown in Fig. 14. The most striking conclusion is that these quantities are virtually independent of Mach number, and only slightly dependent on γ . On the other hand, results presented in Fig. 15 show that the temperature depends strongly on Mach number and γ , with higher values associated with higher Mach numbers and larger γ , a trend clearly revealed by inspection of equation (28).

A useful quantity for characterizing the location of the bow shock wave is the standoff distance Δ at the nose of the magnetosphere. This distance is controlled to a large degree by mass conservation considerations, since the mass flow passing between the magnetosphere and the bow wave at any station must match that crossing the bow wave inside that station. More specifically, the standoff distance at high Mach numbers is determined almost entirely by the density ratio ρ_1/ρ_∞ across the bow wave on the stagnation streamline. The latter is related to the free-stream Mach number and the ratio of specific heats according to the following expression:

$$\frac{\rho_1}{\rho_\infty} = \frac{(\gamma + 1)M_\infty^2}{(\gamma - 1)M_\infty^2 + 2} \quad (29)$$

The variation of standoff distance with ρ_1/ρ_∞ is presented for a wide range of values for γ and free-stream Mach number M_∞ in Fig. 16. As

previously shown in an aerodynamic context by Seiff⁽³⁴⁾ and Inouye⁽³⁵⁾, this distance varies nearly linearly with ρ_{∞}/ρ_1 over a wide range of conditions. With the standoff distance Δ normalized by the distance D from the center of the earth to the nose of the magnetosphere, the following simple empirical formula emerges

$$\Delta/D = 1.1\rho_{\infty}/\rho_1 \quad (30)$$

In order to illustrate further details of supersonic flow of a compressible gas past the magnetosphere, an experiment was conducted in the Ames Research Center, Supersonic Free Flight Wind Tunnel, by Donn Kirk in which shadowgraph photographs were taken of a metal model of the magnetosphere in flight at Mach numbers between about 4.5 and 5 through argon. In normal use of this facility, models are fired from a 50 caliber light-gas gun upstream through an elongated test section of an otherwise normal supersonic wind tunnel. The working fluid normally employed is air, but other gases can be used for a more limited range of test conditions that can be reached by shooting the models into stationary gas. In other words, the wind tunnel is only used as a tank to contain the gas into which the model is fired as in a conventional ballistics range. Since the relative velocity between any given projectile and the gas is thus limited by the allowable muzzle velocity, the maximum Mach number that can be attained depends primarily on the speed of sound in the gas in the test section. By selecting argon as the gas, it is possible to obtain a value of $5/3$ for γ and a low enough speed of sound that Mach numbers as high as 4.5 or 5 can be achieved by firing the projectile into stationary gas. Although these conditions are not identical with those experienced by the

actual magnetosphere past which flows ionized hydrogen at Mach numbers between, say, 5 and 12 or more, they are sufficiently close with respect to the two most important parameters of the present analysis, namely γ and M_∞ , that the results should be useful and instructive.

The model itself must be of finite length and axisymmetric to permit firing in the gun. In accordance with these requirements and in order to facilitate comparison with theoretical results, the model was contoured to the shape described by the equatorial trace of the boundary of the magnetosphere calculated by Spreiter and Hyett⁽³⁶⁾ and Spreiter and Summers⁽³⁷⁾ using a modified version of the Chapman-Ferraro theory in which the boundary condition given here by equation (10) is replaced by a related equation in which the left-hand side is equal to $p_s + p_d \cos^2 \psi$ rather than simply $p_d \cos^2 \psi$ where ψ represents the angle between the directions of the free-stream velocity vector and the normal to the magnetosphere boundary and $p_d = K \rho_\infty v_\infty^2$. Results were given for many different values for the ratio p_s/p_d ; that selected for the experiment is $p_s/p_d = 0.1$. The forward, or sunward, portion of the resulting magnetosphere is very similar, although not identical, to that for $p_s = 0$ used in Figs. 5 through 16. It follows from the basic rules of subsonic and supersonic flow that the location of the bow wave and details of the flow around the forward part of the magnetosphere are very nearly the same whether $p_s/p_d = 0$ or 0.1. The value for this parameter has a profound influence on the shape of the rear of the magnetosphere, however, and details of the flow may be expected to differ correspondingly in this region.

In the photograph of Fig. 17, the Mach number is 4.65; the equivalent position of the earth is represented by the small white circular disc superposed on the opaque model magnetosphere, and the small pointed spike on the downstream side of the magnetosphere is to help identify the orientation of the model as it flies through the test section. This particular photograph was taken with a focussing shadowgraph system which has the property of portraying the shock wave with good resolution, but at the sacrifice of most other details of the flow. Most of the scattered isolated details that are, in fact, visible in the photograph are without geophysical meaning and are the result of damage to the viewing windows caused by impacting models and their fragments in the course of years of use of the facility.

The photograph shown in Fig. 17 is duplicated in Fig. 18 with a superposed line indicating the calculated position for the bow shock wave associated with flow at $M_\infty = 4.65$ of a perfect gas of $\gamma = 5/3$ past a body having the same shape as the magnetosphere model. The accuracy with which the calculation procedures employed in this paper can predict the location of the bow shock wave is illustrated by the essentially perfect agreement with the results illustrated in the shadowgraph.

More details of the flow field can be made visible by photographing the model with an ordinary shadowgraph system rather than the focussing system used to obtain Figs. 17 and 18. A shadowgraph of the same model taken with such a system at a station somewhat farther along in its flight where it had decelerated to a Mach number of 4.50 is shown in Fig. 19. Although the thickness of the bow wave is exaggerated when

viewed through the simple optical system of the ordinary shadowgraph equipment, other details are made visible that are not revealed when viewed through the focussing system. In particular, one may see the characteristic or Mach waves between the forward part of the model and the bow wave in the region where the local velocities are supersonic. Since the model is convex, these waves must be rarefaction waves. They extend outward from the model into the stream until they intersect the bow wave. Comparison with the calculated locations of Mach waves and streamlines presented in Figs. 5 and 9 shows that the faint discontinuity surfaces that extend downstream from the points of intersection of the rarefaction waves and the bow wave are streamlines rather than reflected compression or expansion waves. Any reflected waves that might be present are too weak to be visible in the photographs. Prominently visible in this photograph is the wake of the projectile extending far downstream from the model. The general characteristics of the wake visible in this shadowgraph are similar to those portrayed in many sketches that have been drawn of the flow around the earth's magnetosphere. Recent results from IMP-1 satellite⁽³⁾ provide new insight into the nature of the magnetosphere tail, however, by establishing the existence of a neutral surface separating antisolar directed fields in the southern half of the earth's magnetic tail and solar directed fields in the northern half of the tail. The electrical current that flows in the neutral surface serves to prevent the magnetosphere tail from contracting in cross-section area with increasing distance from the earth and to maintain the tail in a more or less cylindrical configuration for great distances from the earth. For this

reason, certain details of the flow in the vicinity of the wake illustrated in Fig. 19 probably have little relevance with respect to the flow of the solar wind past the earth. They may very well have considerable relevance, however, to the flow past a large and slightly magnetized object such as, possibly, the moon or Venus.

There remains the question as to how accurately the simple Newtonian pressure formula given by $p = p_d \cos^2 \psi$ provides the variation of pressure along the magnetosphere boundary. This can be checked in the present applications by simply comparing the pressure so determined with that indicated by the detailed gasdynamic calculations. The results of such a comparison are assembled in Fig. 20 for the cases included in Figs. 5 through 15. It can be seen that the simple Newtonian expression provides a generally good approximation over most of the magnetosphere boundary of interest in the present studies. The agreement is particularly good over the portion of the magnetosphere along which the flow is subsonic. No significant changes are to be expected, therefore, in the shape of the nose portion of the bow wave due to the use of a more accurate and necessarily more complicated calculation of the pressure. The Newtonian pressure formula does, however, underestimate the pressure somewhat along the flanks of the magnetosphere, indicating that a revised calculation using the gasdynamic pressure distribution would lead to a slightly slimmer magnetosphere. Since the magnetic pressure against which the gas pressure is balanced according to the discussion following equation (9) is approximately proportional to the inverse sixth power of the distance from the center of the earth, the resulting change in the magnetosphere

shape would be expected to be small. A point of equal interest displayed by these results is the lack of significant variation of the pressure distribution with changes in M_∞ and γ over the range of conditions included in the calculations.

The pressure at the nose of the magnetosphere provided by the detailed calculations agrees, as it must, with the following well known expression for the stagnation pressure at the nose of a blunt obstacle in a supersonic stream⁽³⁸⁾.

$$\frac{p_d}{\rho_\infty v_\infty^2} = \left(\frac{\gamma + 1}{2}\right)^{\frac{\gamma+1}{\gamma-1}} \frac{1}{\gamma[\gamma - (\gamma - 1)/2M_\infty^2]^{1/(\gamma-1)}} \quad (31)$$

This expression is derived by considering the flow to experience a sudden compression as it traverses a normal gasdynamic shock wave followed by an additional gradual isentropic compression as it decelerates to rest at the nose of the obstacle. It simplifies as follows for $\gamma = 2$ or $5/3$.

$$\frac{p_d}{\rho_\infty v_\infty^2} = \begin{cases} \frac{27}{32} \left(\frac{1}{1 - 1/4M_\infty^2}\right) & \text{for } \gamma = 2 \\ \frac{256}{225} \left(\frac{3}{5}\right)^{1/2} \left(\frac{1}{1 - 1/5M_\infty^2}\right)^{3/2} & \text{for } \gamma = 5/3 \end{cases} \quad (32)$$

Since the free-stream Mach number M_∞ is much greater than unity in the present applications, comparison with the Newtonian expression for the pressure at the magnetosphere nose, namely $p_d = K\rho_\infty v_\infty^2$ as indicated in equation (10), reveals that K approaches 0.844 for $\gamma = 2$ and 0.881 for $\gamma = 5/3$. Since equation (27) shows that the distance D to the nose of the magnetosphere is proportional to the inverse sixth root of K , it

follows immediately that the size as well as the shape of the magnetosphere is very insensitive to variations of the Mach number and ratio of specific heats of the solar wind gas.

10. DISTORTION OF THE INTERPLANETARY FIELD

As noted previously, the results presented in the preceding section represent solutions of equations (1), (2) and (4) with the terms containing \underline{H} omitted because of their smallness. Following this procedure, the calculation of the flow field about the magnetosphere is decoupled from the influence of the magnetic field, and the calculation of the deformation of the magnetic field is deferred to a subsequent step that depends on the solution for the flow field. Once the latter is determined and an orientation for the magnetic field in the incident stream is specified, the calculation of the magnetic field surrounding the magnetosphere can be achieved by integration of the previously unused relations of equation (1), namely $\text{curl} (\underline{H} \times \underline{y}) = 0$ and $\text{div} \underline{H} = 0$. The latter are commonly interpreted as indicating the magnetic field lines move with the fluid. This convenient interpretation leads to a straightforward, although tedious, calculation in which the vector distance from each point on an arbitrarily selected field line to its corresponding point on an adjacent field line in the downstream direction is determined by numerically integrating $\int \underline{y} dt$ over a fixed time interval δt . This procedure leads in general to field lines that are curved in space.

Simplicity may be achieved at the expense of completeness by confining attention to the plane containing the velocity and magnetic field vectors in the incident stream. Since the magnetosphere has been approximated by an axisymmetric shape, it follows that the resulting field lines

for this case are also confined entirely to the same plane. Results of two such calculations are shown in Fig. 21. Both sets of results are for a free-stream Mach number of 8 and a gas with $\gamma = 5/3$, but no qualitative changes are anticipated if somewhat different values are selected since the velocity field is only slightly influenced by variations of Mach number and specific heat ratio. The magnetic field in the incident stream is inclined at 90° to the direction of the velocity vector in the left portion of Fig. 21, and 45° in the right portion. The corresponding results for 0° inclination are not presented, but can be visualized easily because the field lines for that case are aligned everywhere with the streamlines.

These results clearly show how the magnetic field lines bend discontinuously as they pass through the bow wave at any angle except a right angle, and then curve in a continuous manner throughout the entire region between the bow wave and the magnetosphere. The discontinuous bend at the shock wave is, moreover, always in the direction that preserves the sign of the tangential component of the field, as is required for all physically relevant hydromagnetic shock waves. It may be seen that the field lines illustrated in Fig. 21 are all draped around the nose of the magnetosphere. This is characteristic of the results for all relative orientations, except perfect alignment, of the magnetic field and velocity vectors for the special plane for which these results are presented. Outside of this plane, however, the field lines drift around the nose with the flow and deform into three-dimensional or spatial curves. The strong constraint imposed on the magnetic field by the stagnation point at the magnetosphere nose is thus greatly reduced, and the field lines may be anticipated to remain much straighter than illustrated in Fig. 21.

REFERENCES

1. IG Bulletin 84, Trans. American Geophys. Union 45, 501 (1964).
2. N. F. NESS, NASA Goddard Space Flight Center Report X-612-64-392 (1964).
3. N. F. NESS, J. Geophys. Res. 70, 517 (1965).
4. N. F. NESS, C. S. SCEARCE and J. B. SEEK, J. Geophys. Res. 69, 3531 (1964).
5. W. I. AXFORD, H. E. PETSCHKE and G. L. SISCOE, J. Geophys. Res. 70, 1231 (1965).
6. A. J. DESSLER and R. D. JUDAY, Planet. Space Sci. 13, 63 (1965).
7. W. I. AXFORD, J. Geophys. Res. 67, 3791 (1962).
8. P. J. KELLOGG, J. Geophys. Res. 67, 3805 (1962).
9. J. W. FREEMAN, J. A. VAN ALLEN and L. J. CAHILL, J. Geophys. Res. 68, 2121 (1963).
10. J. R. SPREITER and W. P. JONES, J. Geophys. Res. 68, 3555 (1963).
11. L. Lees, AIAA Jour. 2, 1576 (1964).
12. R. H. LEVY, H. E. PETSCHKE and G. L. SISCOE, AIAA Jour. 2, 2065 (1964).
13. G. CHEW, M. L. GOLDBERGER and F. E. IOW, Proc. Roy. Soc. A236, 112 (1956).
14. L. D. LANDAU and E. M. LIFSHITZ, Electrodynamics of Continuous Media, p. 213, Pergamon Press, Oxford-New York (1960).
15. K. O. FRIEDRICHS and H. KRANZER, AEC Computing and Applied Mathematics Center, Univ. Report NYO-6486 MH-8 (1958).
16. G. J. F. MacDonald, Space Physics, (Eds. D. P. LeGalley and A. Rosen), p. 474. John Wiley and Sons, New York (1964).

17. J. E. ANDERSON, Magnetohydrodynamic Shock Waves, M.I.T. Press, Cambridge, Mass. (1963).
18. A. JEFFREY and T. TANIUTI, Non-Linear Wave Propagation With Applications to Physics and Magnetohydrodynamics, Academic Press, New York (1964).
19. A. R. KAMEROWITZ and H. E. PETSCHER, Avco-Everett Res. Lab. Res. Report 185, Everett, Mass. (1964).
20. W. R. SEARS, Rev. Mod. Phys. 32, 701 (1960).
21. I. IMAI, Rev. Mod. Phys. 32, 992 (1960).
22. H. GRAD, Rev. Mod. Phys. 32, 830 (1960).
23. K. TAMADA, Symposium Transsonicum (Ed. K. Oswatitsch), p. 460. Springer-Verlag, Berlin (1960).
24. H. LAMB, Hydrodynamics, Cambridge Univ. Press, Cambridge, Mass. (1932).
25. S. CHAPMAN, Geophysics: The earth's environment, (Eds. C. DeWitt, J. Hieblot and A. Lebeau), p. 371. Gordon and Breach, New York (1963).
26. B. R. BRIGGS and J. R. SPREITER, NASA TR R-178 (1963).
27. J. E. MIDGLEY and L. DAVIS, JR., J. Geophys. Res. 68, 5111 (1963).
28. G. D. MEAD and D. B. BEARD, J. Geophys. Res. 69, 1169 (1964).
29. M. INOUE and H. LOMAX, NASA TN D-1426 (1962).
30. M. D. VAN DYKE, J. Aeron. Sci. 25, 485 (1958).
31. M. D. VAN DYKE and H. D. GORDON, NASA TR R-1 (1959).
32. F. B. FULLER, NASA TN D-791 (1961).
33. H. LOMAX and M. INOUE, NASA TR R-204 (1964).
34. A. SEIFF, Gasdynamics in Space Exploration, p. 19 NASA SP-24 (1962).
35. M. INOUE, AIAA Jour. 3, 172 (1965).

36. J. R. SPREITER and B. J. HYETT, J. Geophys. Res. 68, 1631 (1963).
37. J. R. SPREITER and A. L. SUMMERS, NASA TR R-181 (1963).
38. L. D. LANDAU and E. M. LIFSHITZ, Fluid Mechanics, p. 458. Pergamon Press, London; Addison-Wesley Pub. Co., Reading, Mass. (1959).

FIGURE LEGENDS

- Fig. 1. Normal speed or Friedrichs I diagrams for propagation velocity of weak plane waves.
- Fig. 2. View of coordinate systems.
- Fig. 3. Speed of sound and Alfvén waves in the solar wind.
- Fig. 4. Sketches showing how asymptotic directions of shock waves, rotational discontinuities, and wake can be determined by use of Friedrichs I or II diagrams. (a) Using Friedrichs I diagram for plane waves. (b) Using Friedrichs II diagram for waves from a point disturbance.
- Fig. 5. Streamlines and wave patterns for supersonic flow past the magnetosphere; $M_\infty = 8$, $\gamma = 2$.
- Fig. 6. Density contours for supersonic flow past the magnetosphere; $M_\infty = 8$, $\gamma = 2$.
- Fig. 7. Velocity and temperature contours for supersonic flow past the magnetosphere; $M_\infty = 8$, $\gamma = 2$.
- Fig. 8. Mass flux contours for supersonic flow past the magnetosphere; $M_\infty = 8$, $\gamma = 2$.
- Fig. 9. Streamlines and wave patterns for supersonic flow past the magnetosphere; $M_\infty = 8$, $\gamma = 5/3$.
- Fig. 10. Density contours for supersonic flow past the magnetosphere; $M_\infty = 8$, $\gamma = 5/3$.
- Fig. 11. Velocity and temperature contours for supersonic flow past the magnetosphere; $M_\infty = 8$, $\gamma = 5/3$.

- Fig. 12. Mass flux contours for supersonic flow past the magnetosphere;
 $M_\infty = 8$, $\gamma = 5/3$.
- Fig. 13. Position of bow shock wave for various M_∞ and γ .
- Fig. 14. Variation of density, velocity, and mass flux along the magnetosphere boundary and the downstream side of the bow shock wave for various M_∞ and γ .
- Fig. 15. Variation of temperature along the magnetosphere boundary and the downstream side of the bow shock wave for various M_∞ and γ .
- Fig. 16. Variation of standoff distance with density ratio across bow shock wave on the stagnation streamline.
- Fig. 17. Focussed shadowgraph of model magnetosphere in free flight at Mach number 4.56 through argon ($\gamma = 5/3$).
- Fig. 18. Comparison of calculated and observed positions of bow wave of a model magnetosphere in free flight at Mach number 4.65 through argon ($\gamma = 5/3$).
- Fig. 19. Normal shadowgraph of model magnetosphere in free flight at Mach number 4.50 through argon ($\gamma = 5/3$).
- Fig. 20. Comparison of pressure distribution along the magnetosphere boundary calculated by gasdynamic theory for various M_∞ and γ with that indicated by the simple Newtonian approximation $p = p_d \cos^2 \psi$.
- Fig. 21. Magnetic field in plane of free-stream velocity and magnetic field vectors for supersonic flow past the magnetosphere, $M_\infty = 8$, $\gamma = 5/3$.

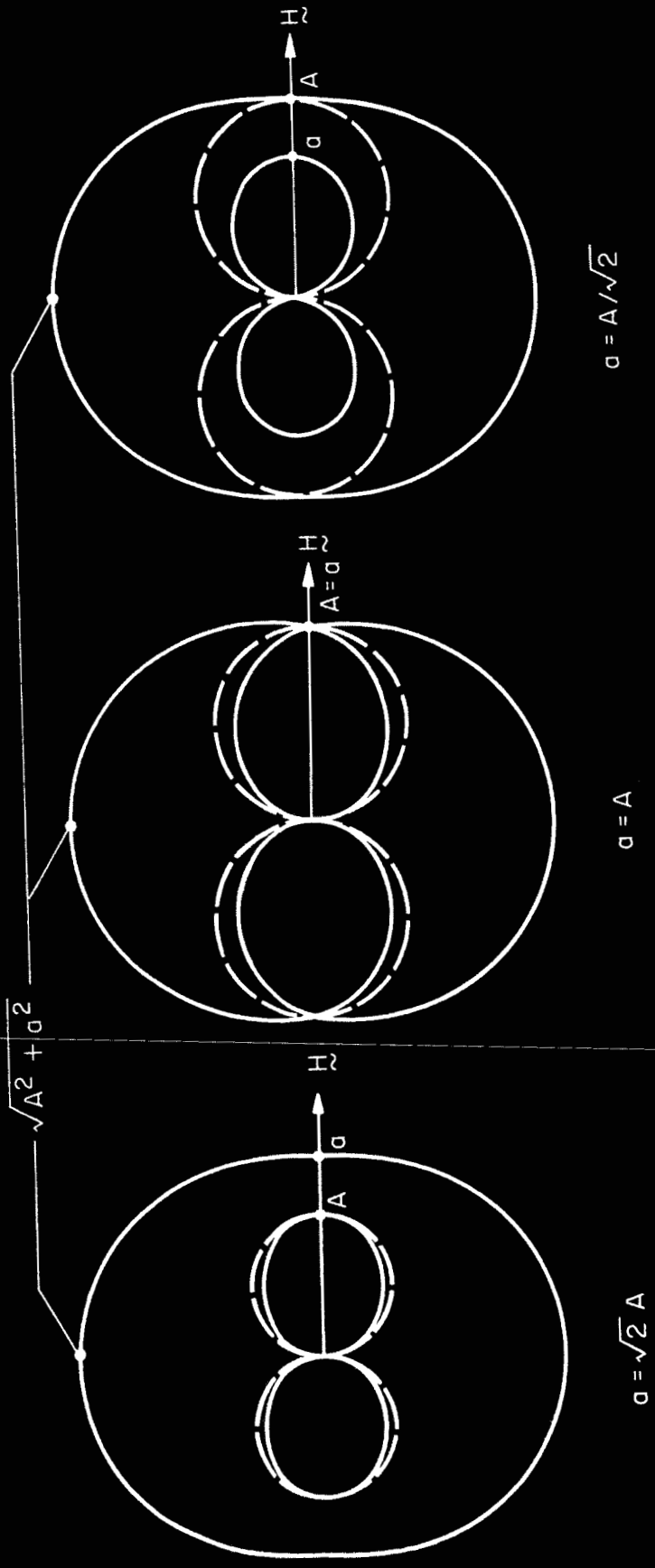


Fig. 1

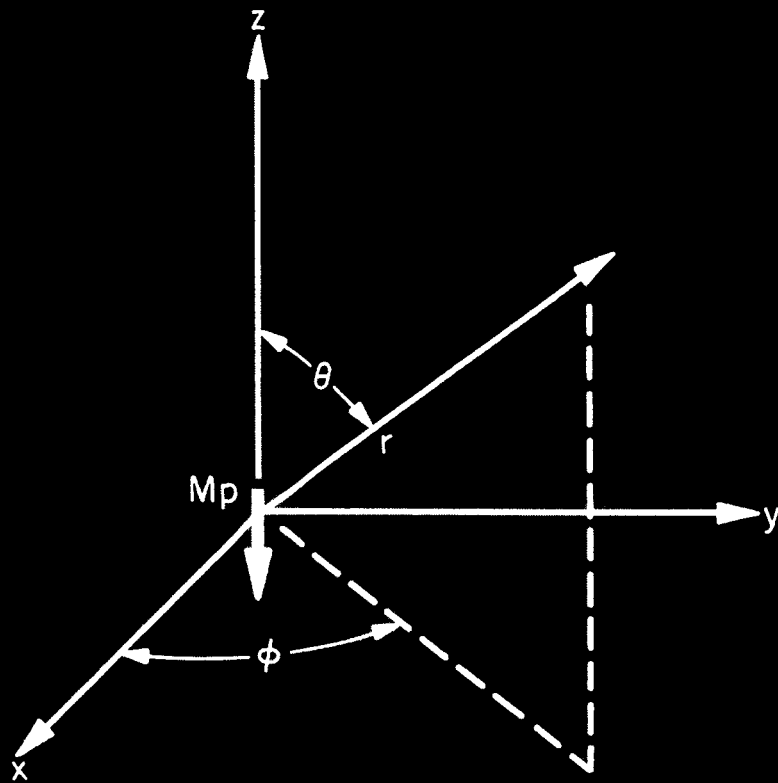


Fig. 2

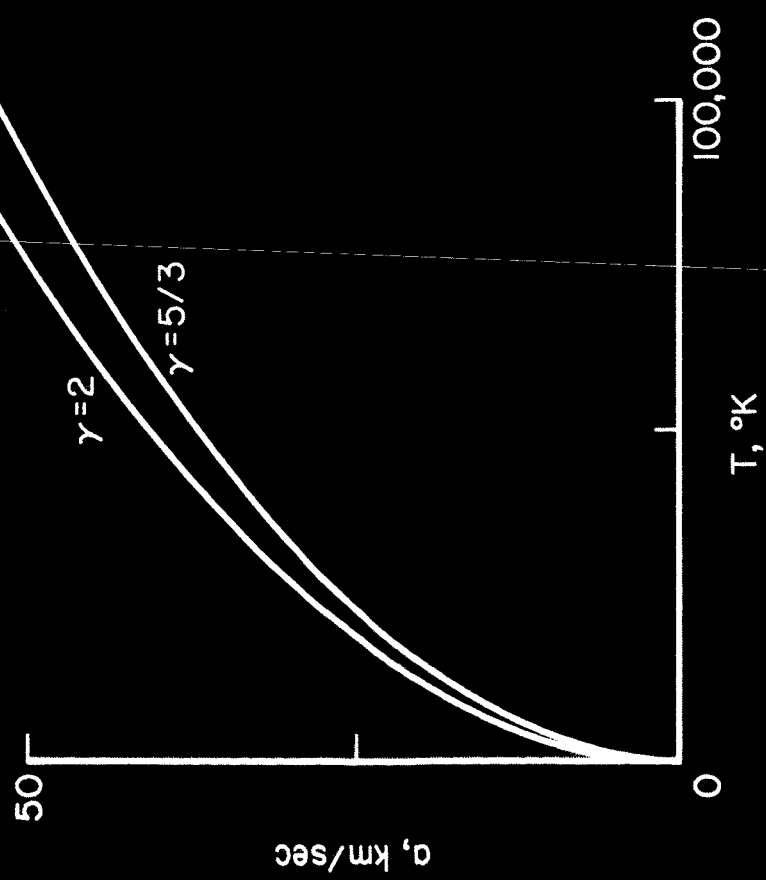
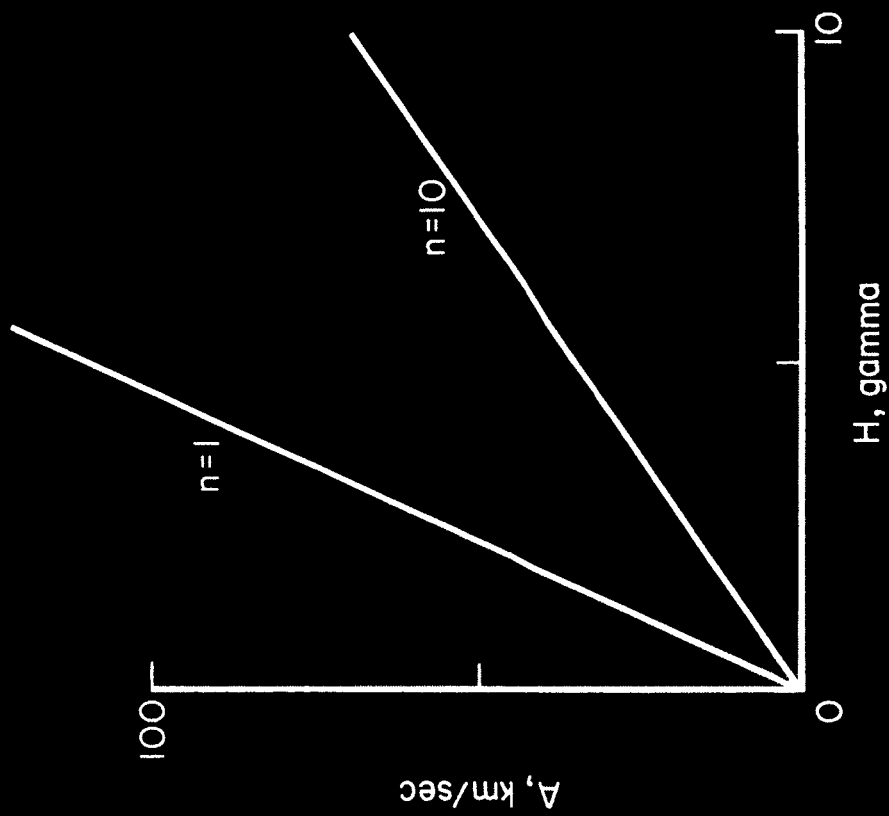


FIG. 3

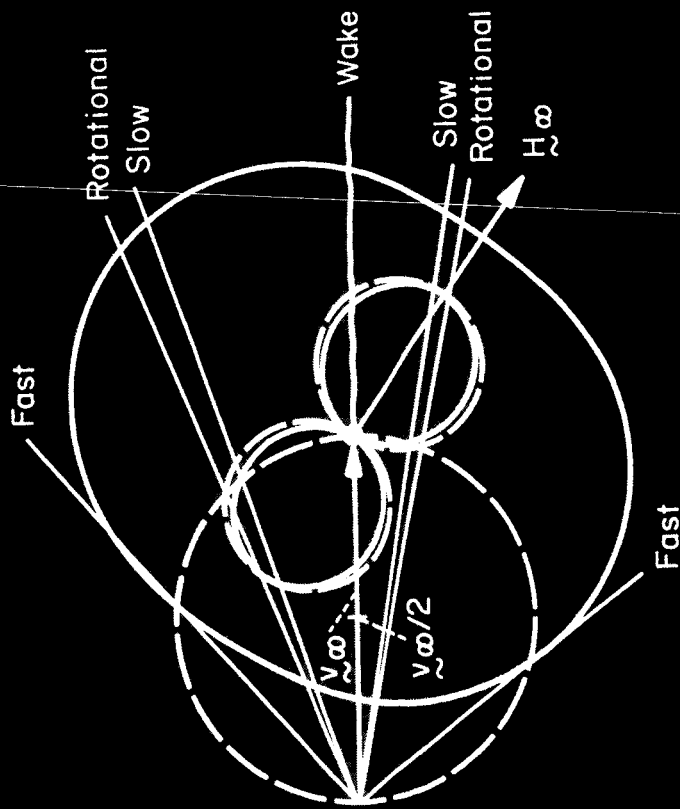
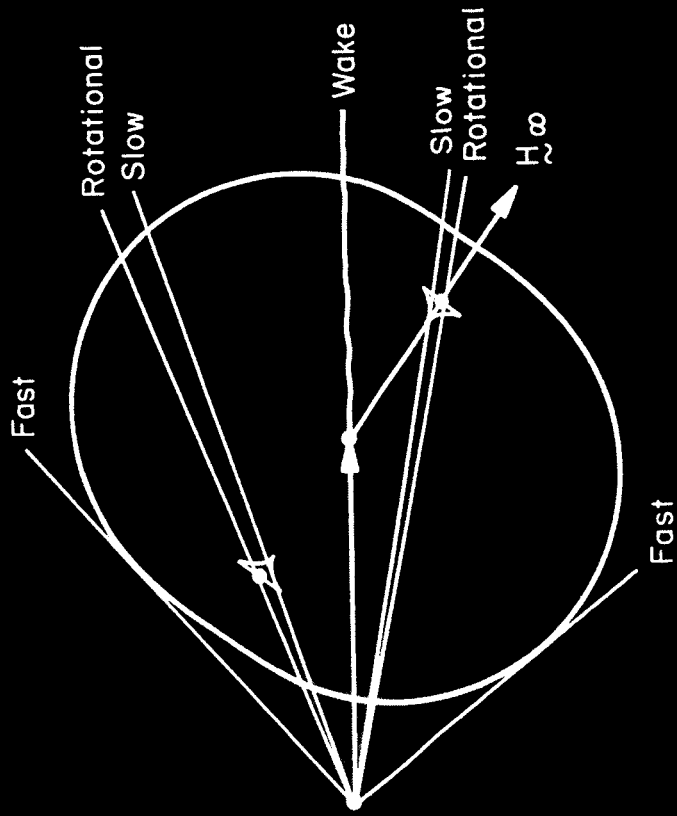


FIG. 1

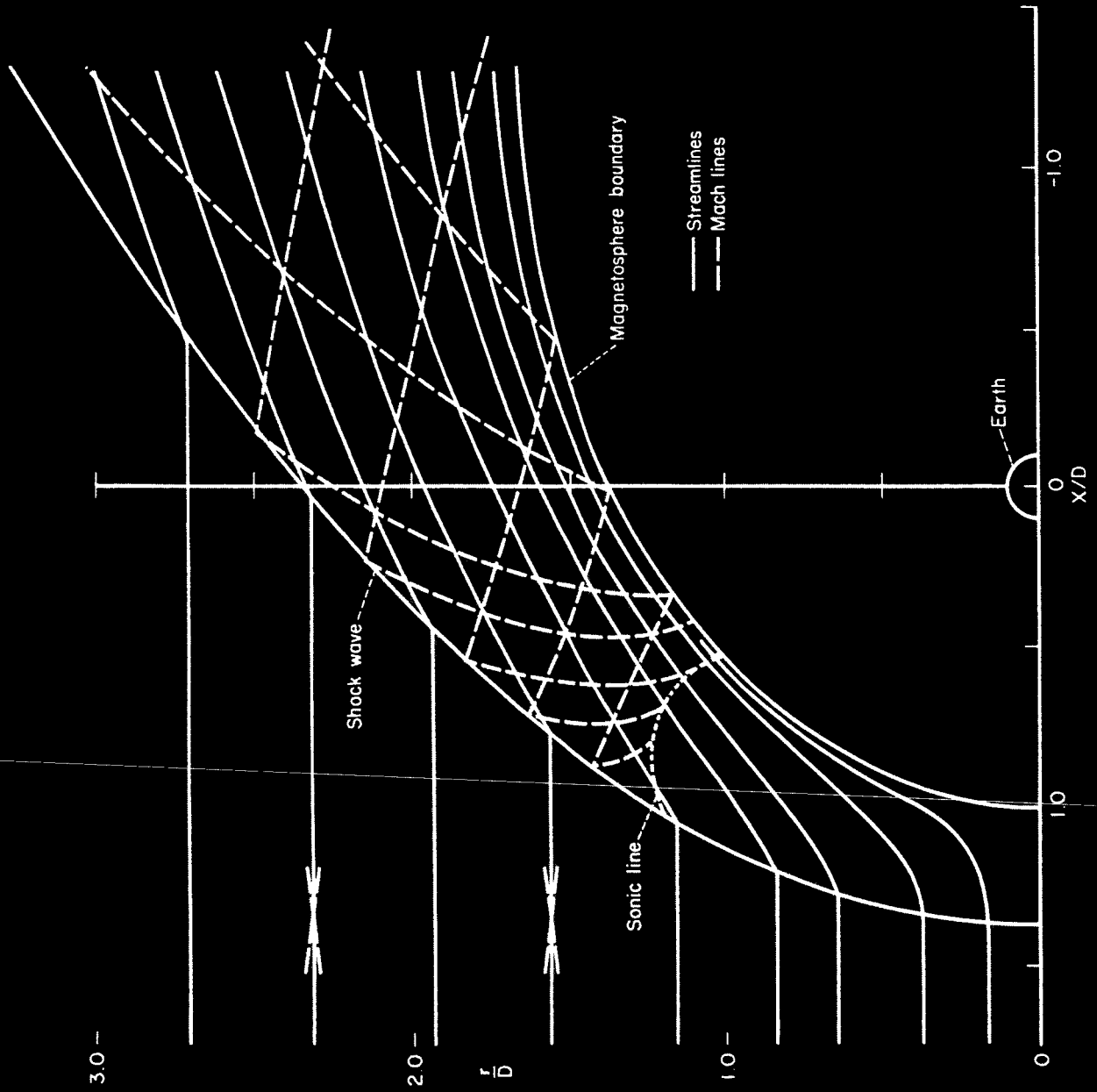


Fig. 5

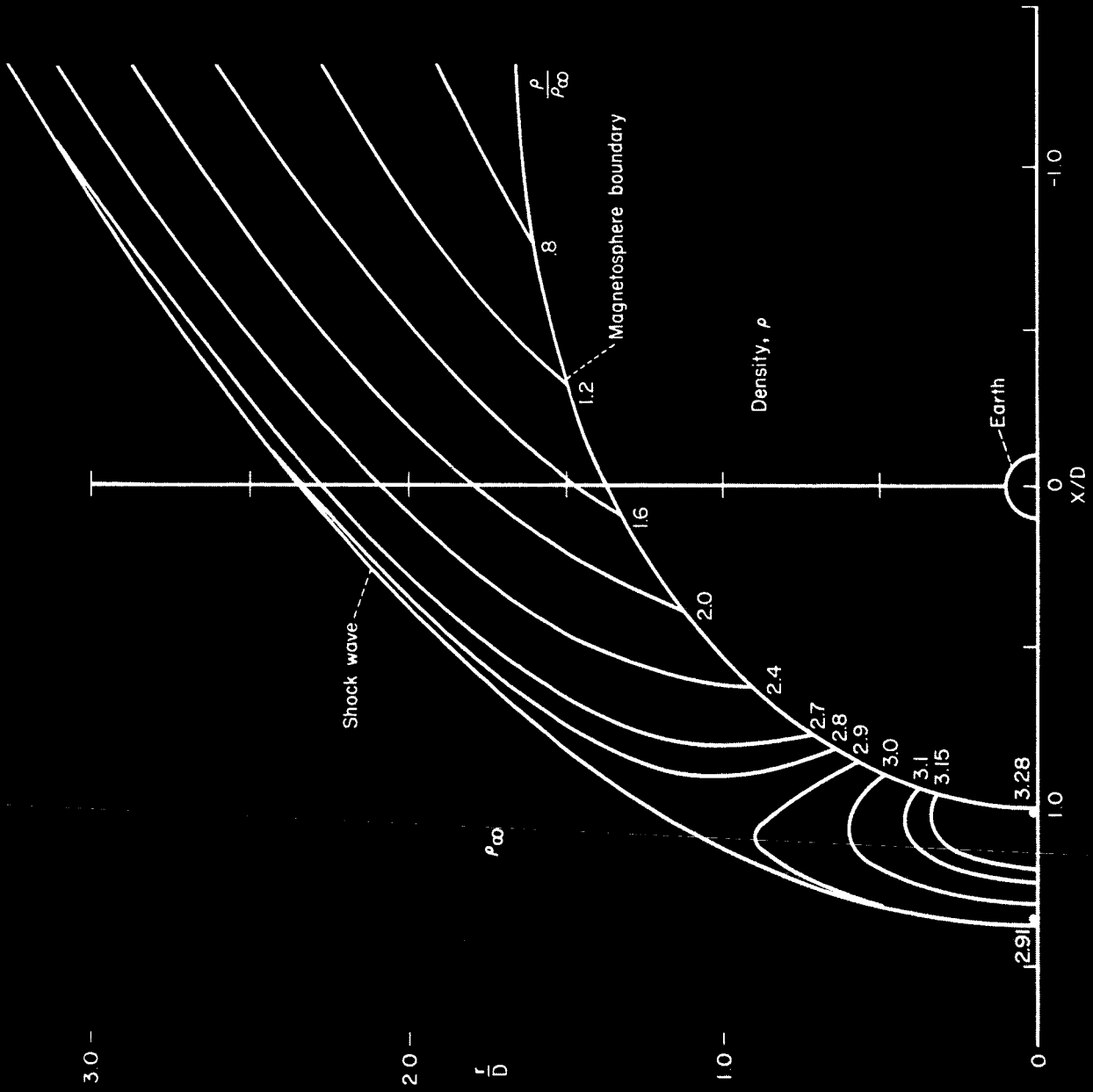


FIG. 6

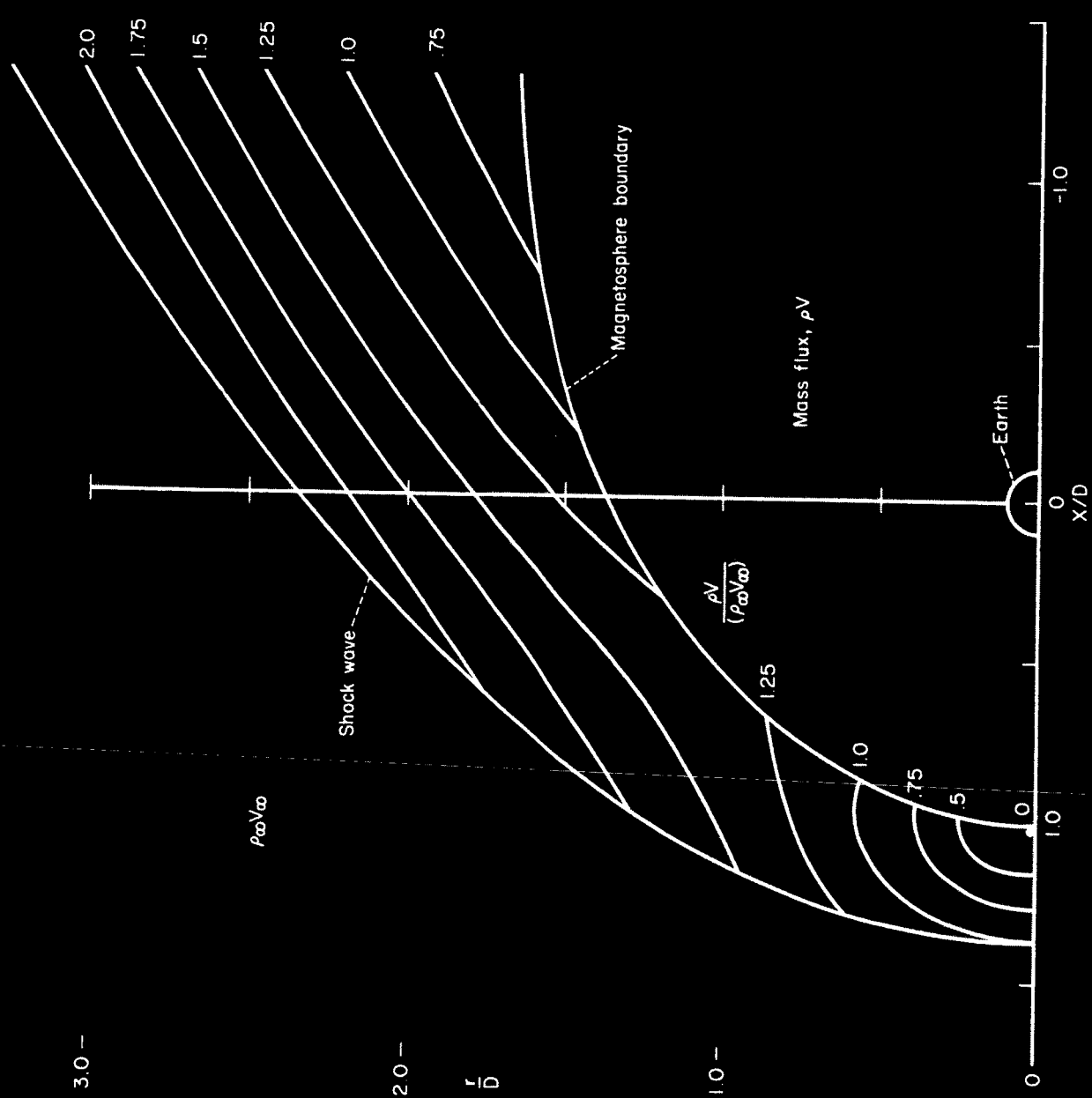


FIG. 6

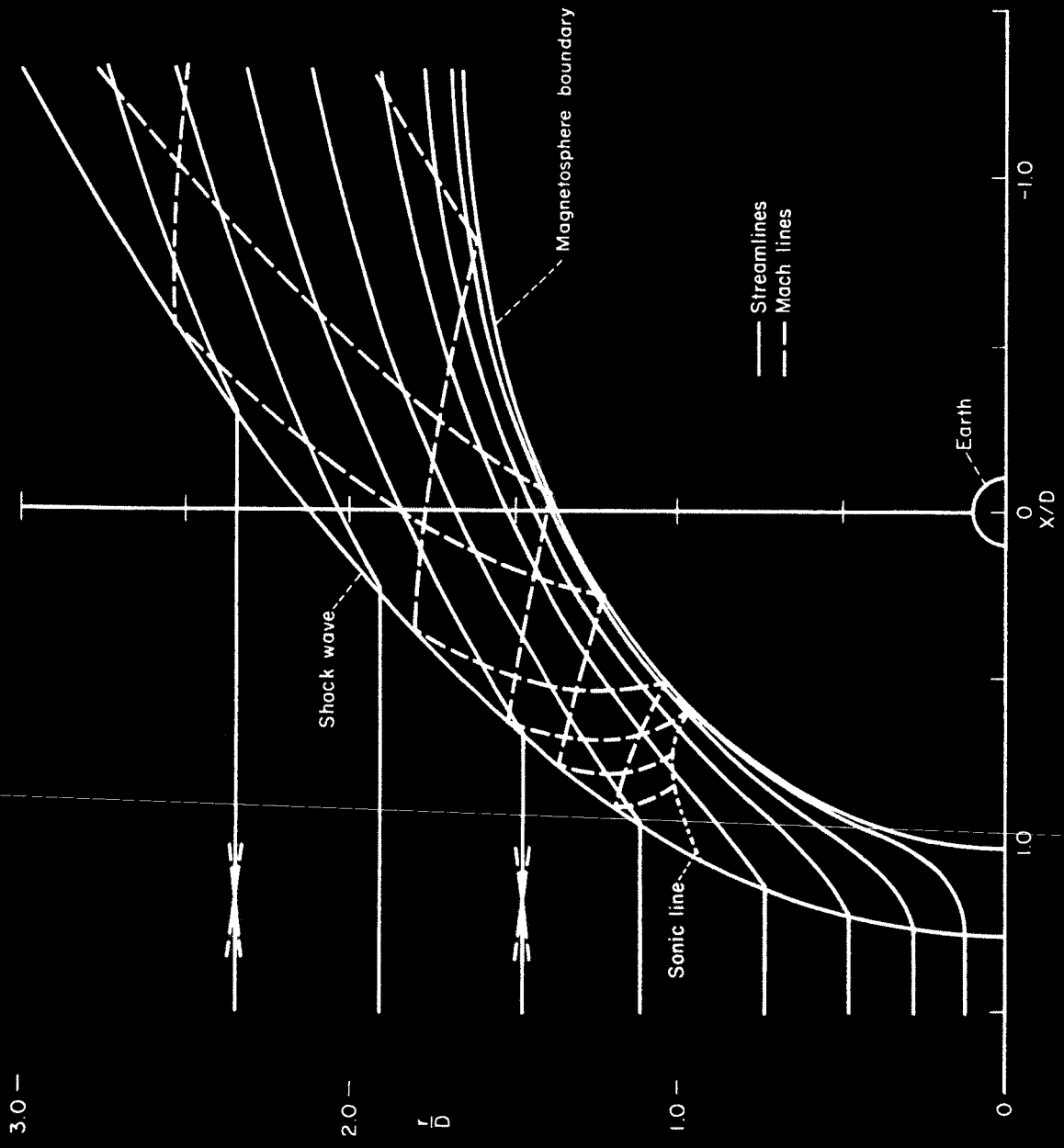


FIG. 9

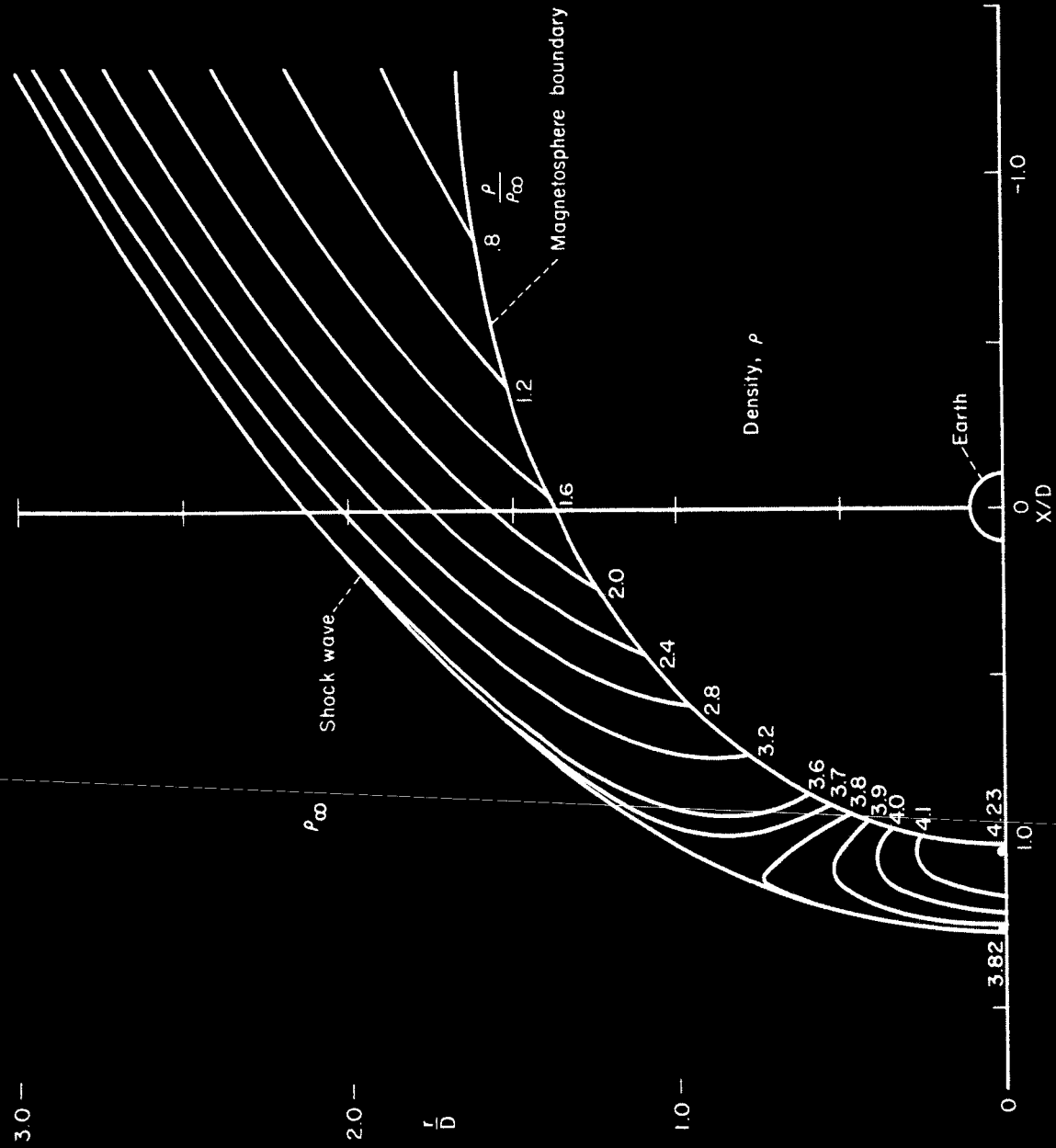


Fig. 10

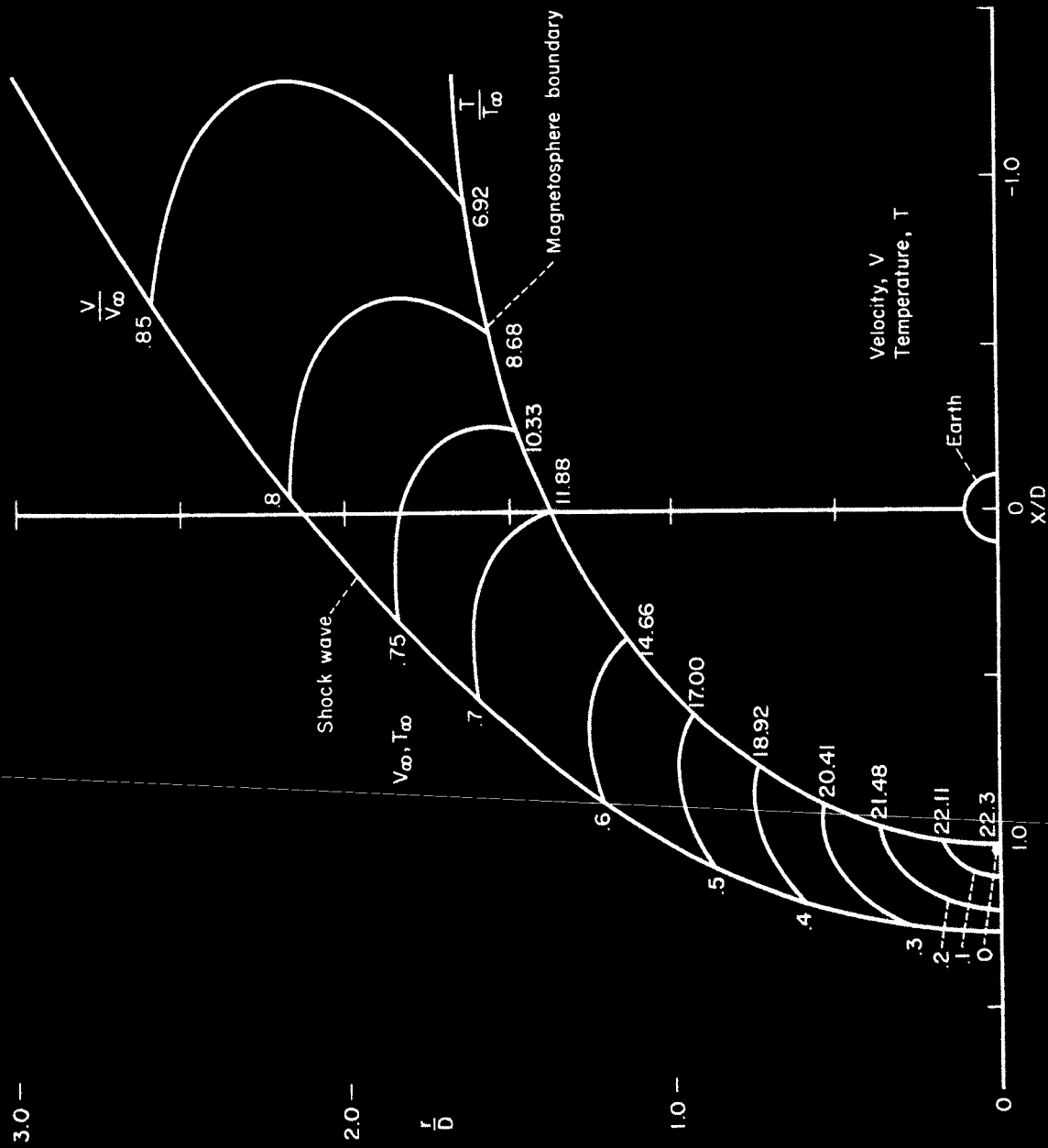


FIG. 11

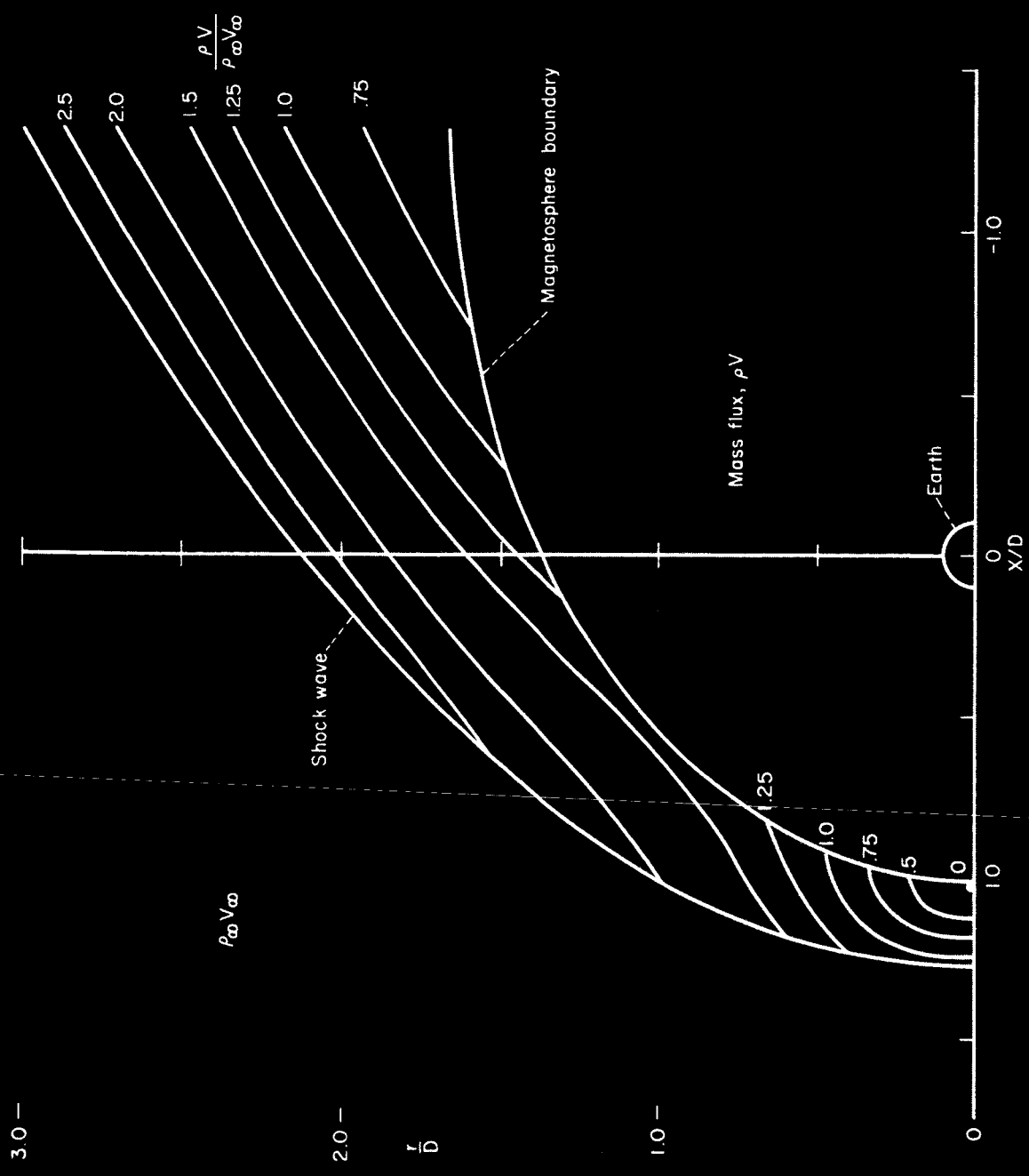


FIG. 12

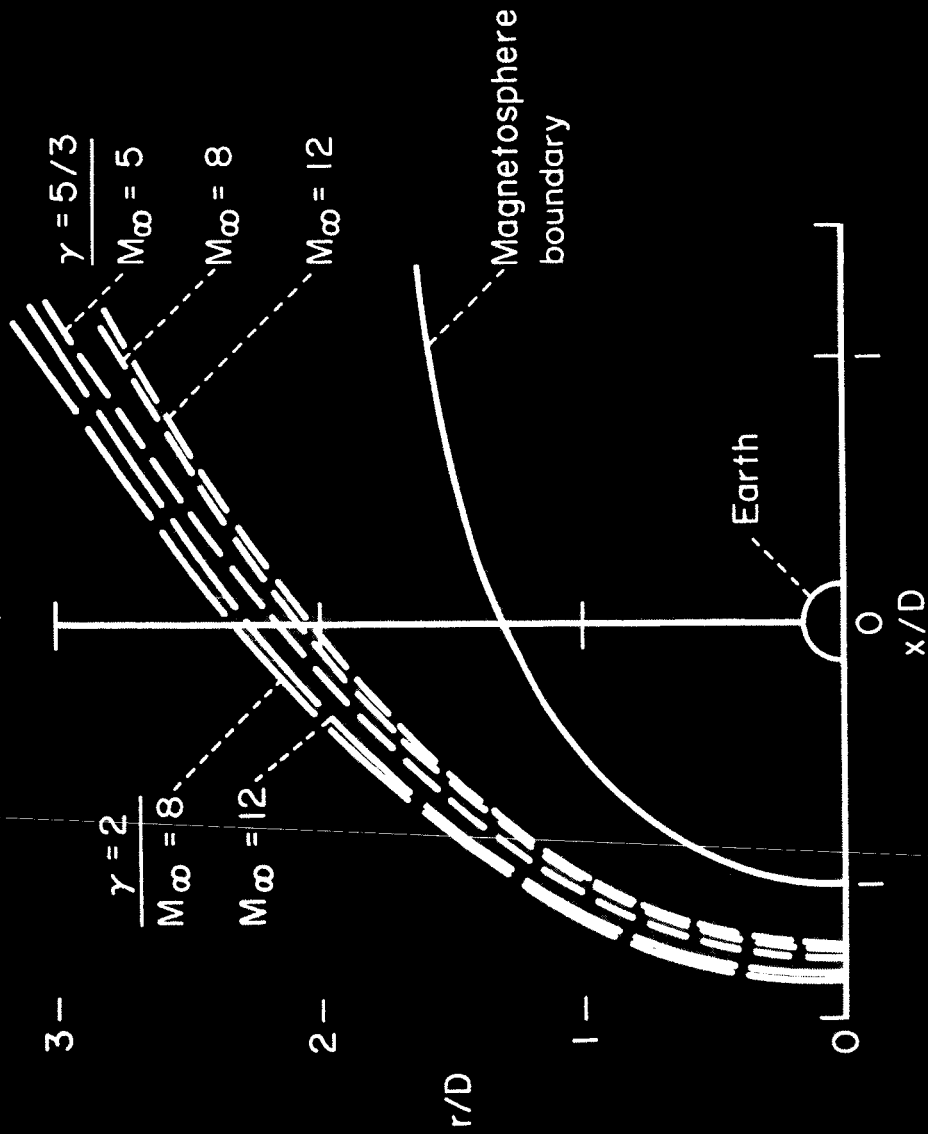


Fig. 13

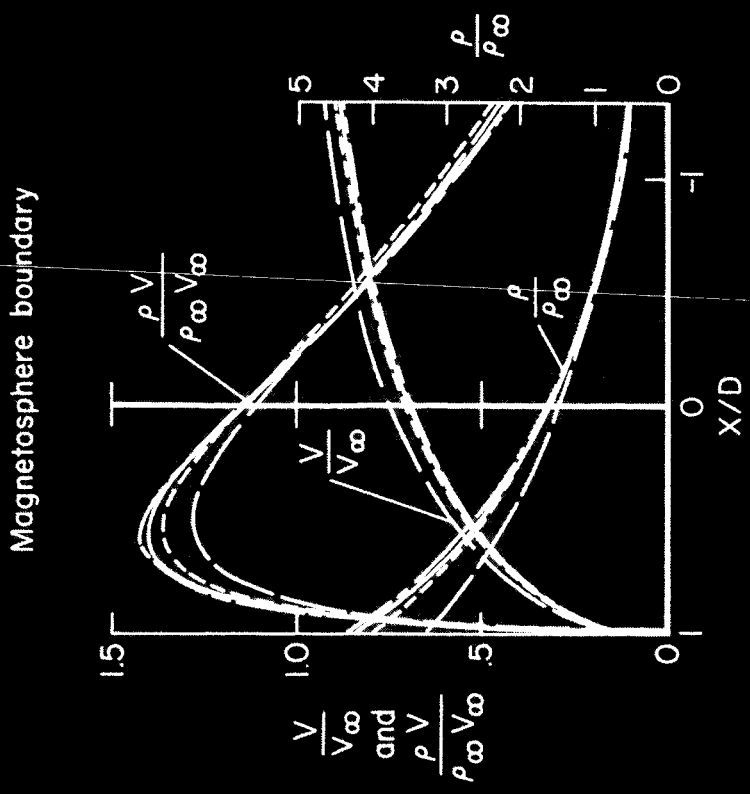
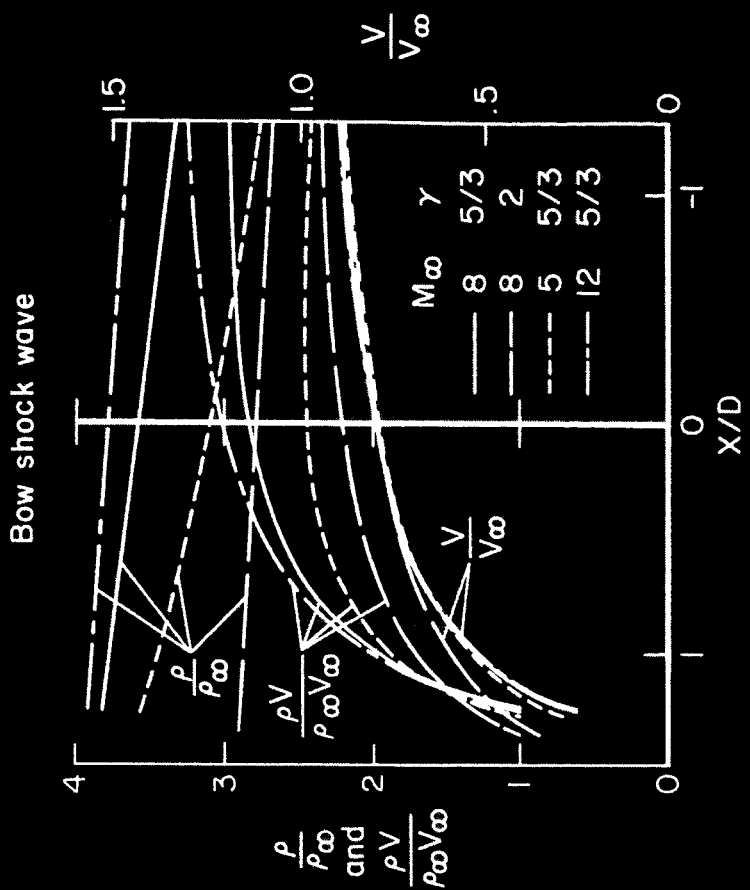


FIG. 14

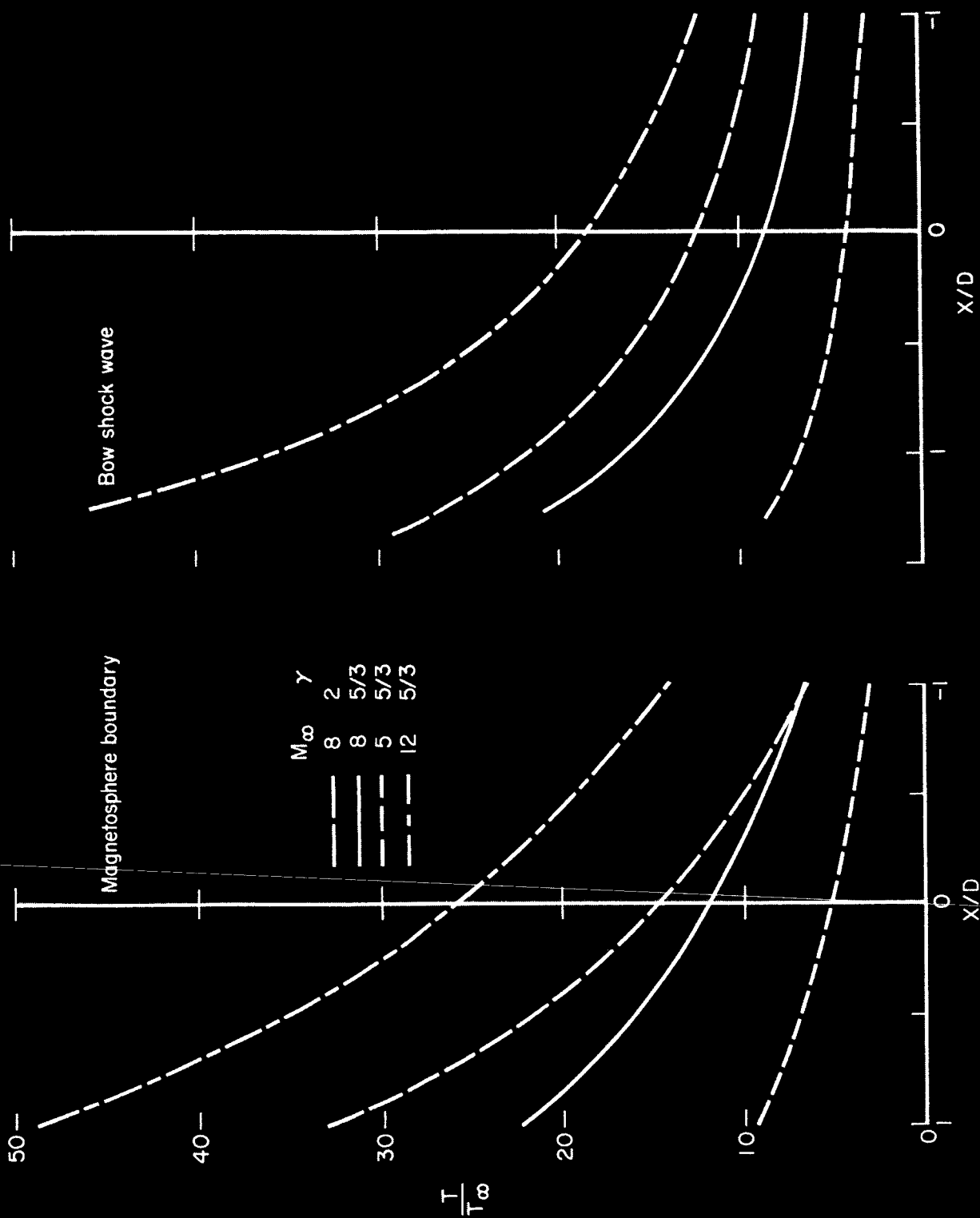


FIG. 15

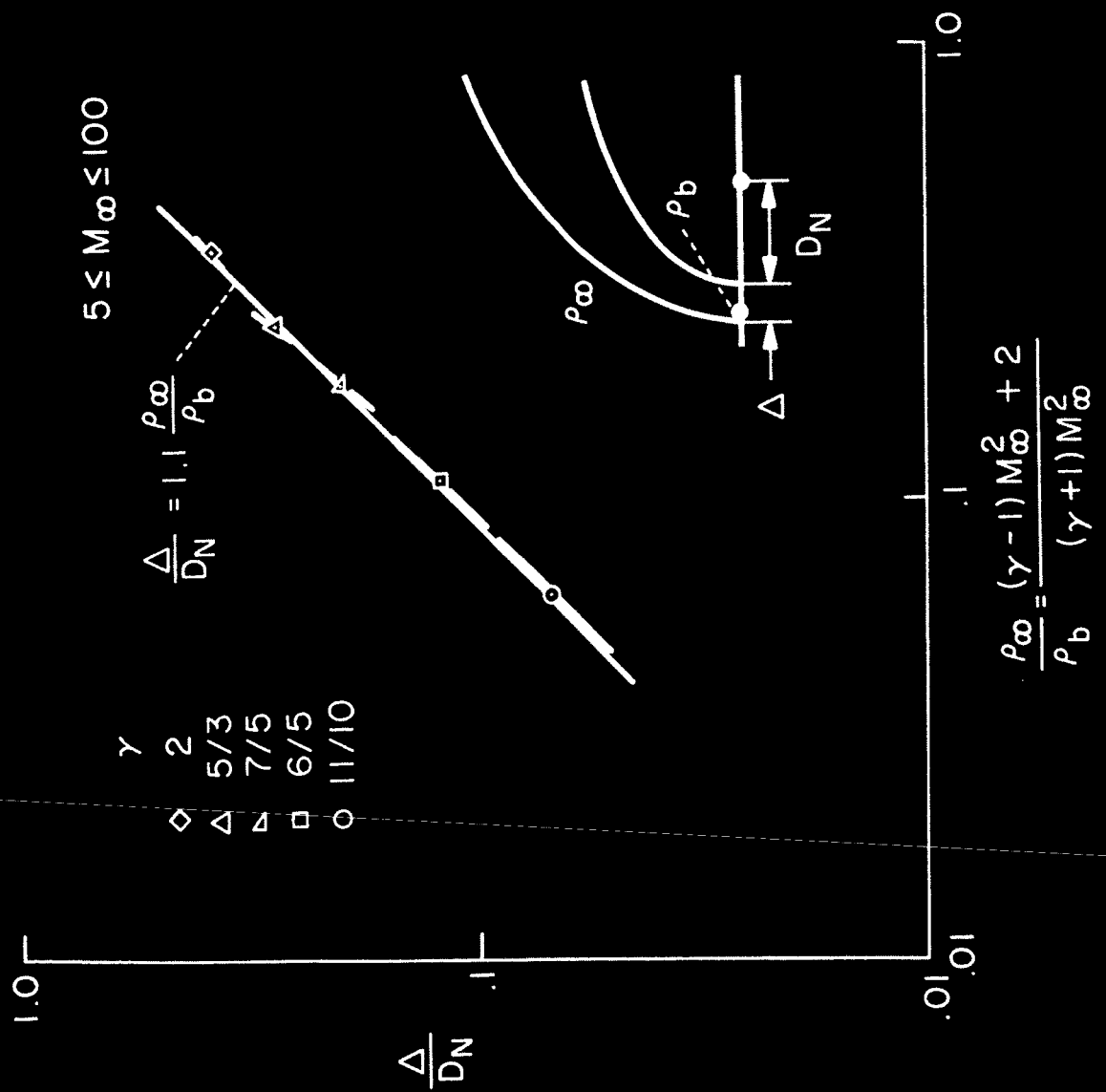


FIG. 16



Fig. 17

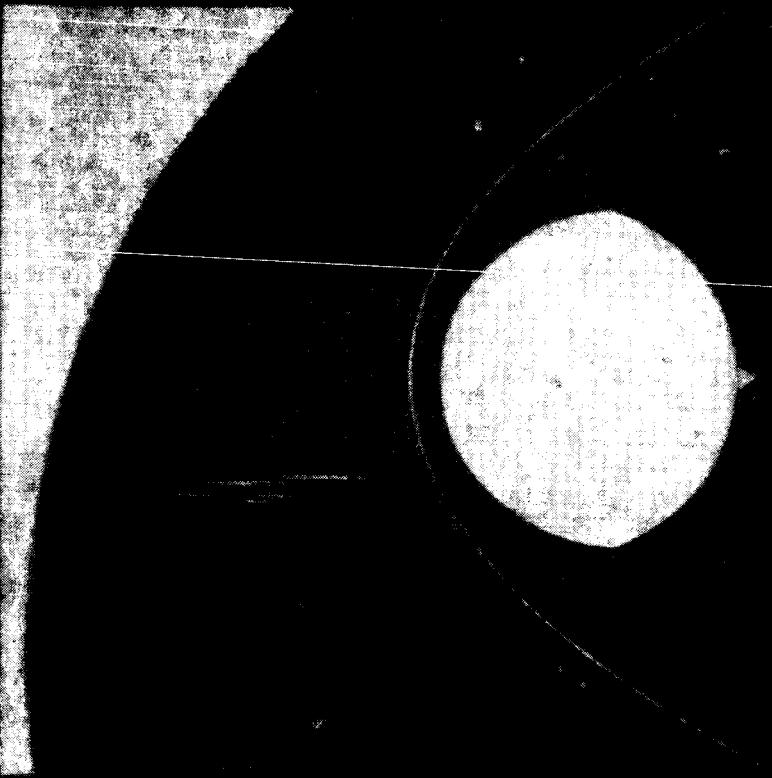


Fig. 18

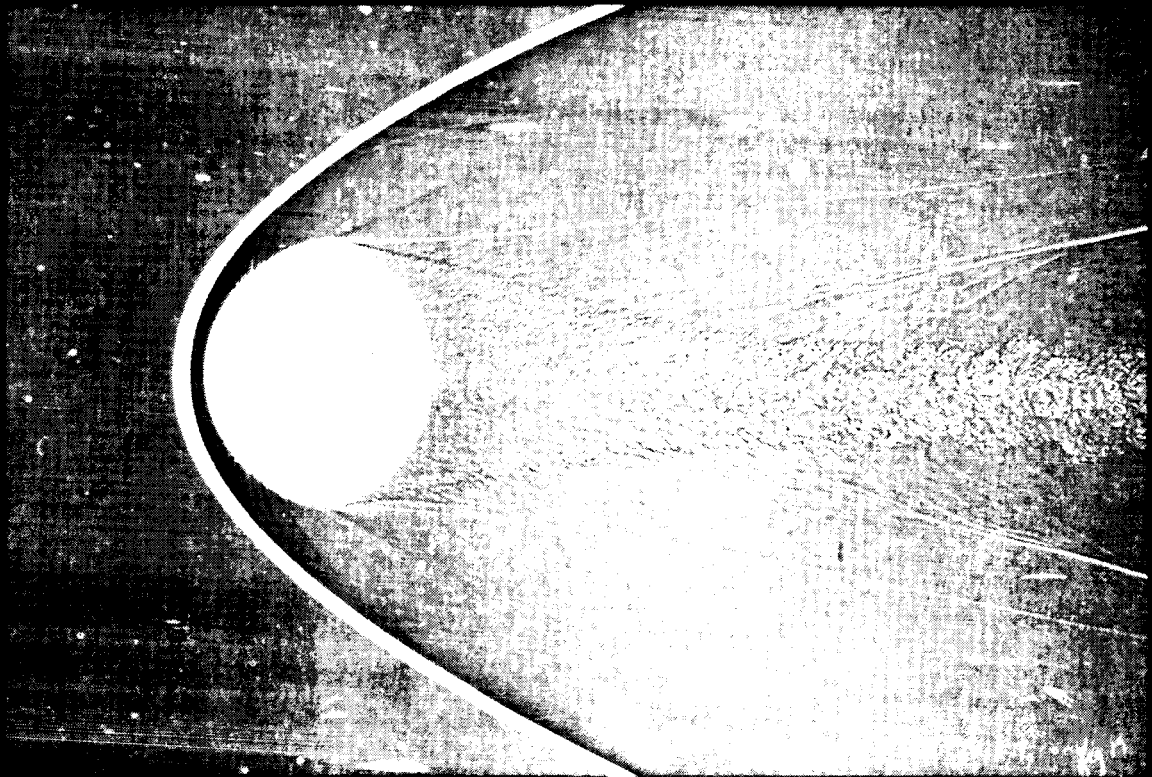
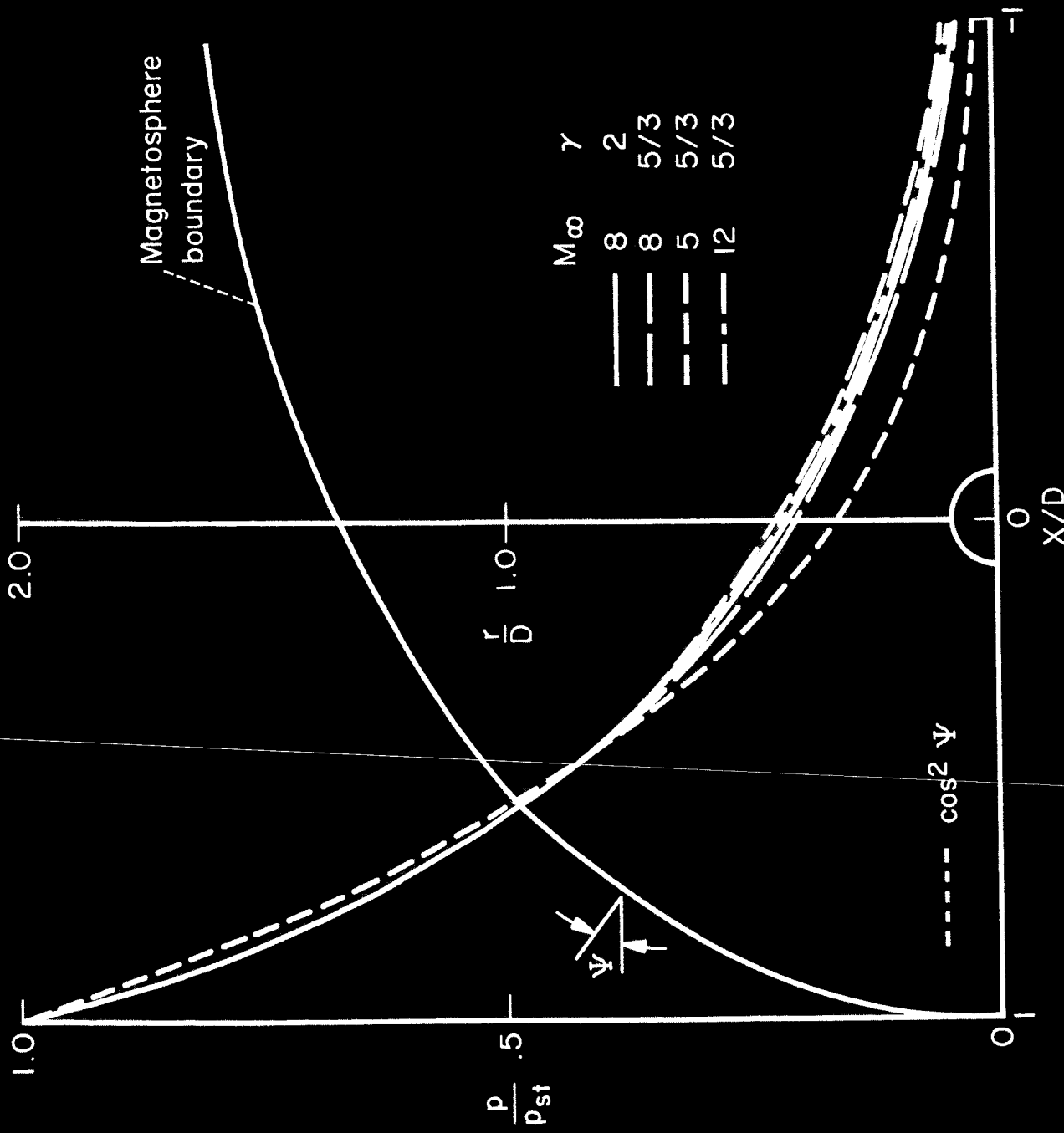


Fig. 19



M_∞	γ
8	2
8	5/3
5	5/3
12	5/3

Fig. 20

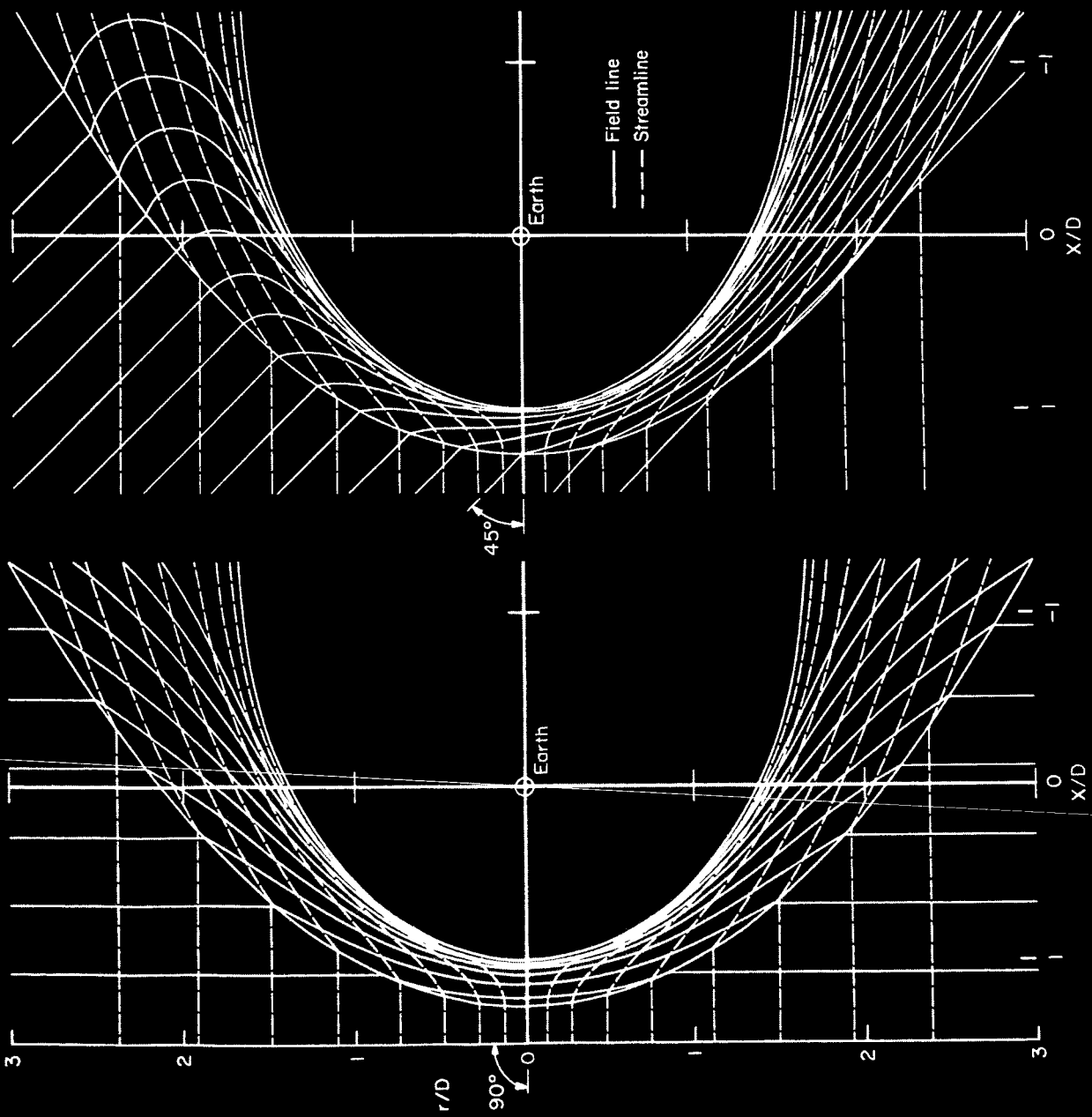


Fig. 21